ARX model-based damage sensitive features for structural damage localization using output-only measurements

ARTICLE *in* JOURNAL OF SOUND AND VIBRATION · AUGUST 2015

Impact Factor: 1.81 · DOI: 10.1016/j.jsv.2015.03.038

3 AUTHORS, INCLUDING:

Dr. Koushik Roy
Indian Institute of Technology Patna
6 PUBLICATIONS **10** CITATIONS

SEE PROFILE

Bishakh Bhattacharya
Indian Institute of Technology Kanpur
64 PUBLICATIONS **157** CITATIONS

SEE PROFILE

Journal of Sound and Vibration 349 (2015) 99–122

Contents lists available at ScienceDirect

Journal of Sound and Vibration

journal homepage: www.elsevier.com/locate/jsvi

ARX model-based damage sensitive features for structural damage localization using output-only measurements

Koushik Roy [a], Bishakh Bhattacharya [b], Samit Ray-Chaudhuri [a,*]

[a] Department of Civil Engineering, Indian Institute of Technology Kanpur, UP 208016, India
[b] Department of Mechanical Engineering, Indian Institute of Technology Kanpur, UP 208016, India

ARTICLE INFO

Article history:
Received 28 February 2014
Received in revised form
3 March 2015
Accepted 19 March 2015
Handling Editor: I. Trendafilova
Available online 16 April 2015

ABSTRACT

The study proposes a set of four ARX model (autoregressive model with exogenous input) based damage sensitive features (DSFs) for structural damage detection and localization using the dynamic responses of structures, where the information regarding the input excitation may not be available. In the proposed framework, one of the output responses of a multi-degree-of-freedom system is assumed as the input and the rest are considered as the output. The features are based on ARX model coefficients, Kolmogorov–Smirnov (KS) test statistical distance, and the model residual error. At first, a mathematical formulation is provided to establish the relation between the change in ARX model coefficients and the normalized stiffness of a structure. KS test parameters are then described to show the sensitivity of statistical distance of ARX model residual error with the damage location. The efficiency of the proposed set of DSFs is evaluated by conducting numerical studies involving a shear building and a steel moment-resisting frame. To simulate the damage scenarios in these structures, stiffness degradation of different elements is considered. It is observed from this study that the proposed set of DSFs is good indicator for damage location even in the presence of damping, multiple damages, noise, and parametric uncertainties. The performance of these DSFs is compared with mode shape curvature-based approach for damage localization. An experimental study has also been conducted on a three-dimensional six-storey steel moment frame to understand the performance of these DSFs under real measurement conditions. It has been observed that the proposed set of DSFs can satisfactorily localize damage in the structure.

1. Introduction

Recent advances in sensor technology and damage detection algorithms show a tremendous potential to overcome the difficulties associated with manual inspections. From last couple of decades, numerous methodologies for system identification have been developed successfully in the area of structural health monitoring. These methods include time domain techniques as well as frequency domain approaches using input–output or output-only measurements. Different algorithms are proposed to detect, quantify, and localize damage for a given structure with various levels of efficiency.

* Corresponding author. Tel.: +91 512 259 7267; fax: +91 512 259 7395.
E-mail addresses: koushik@iitk.ac.in (K. Roy), bishakh@iitk.ac.in (B. Bhattacharya), samitrc@iitk.ac.in (S. Ray-Chaudhuri).

http://dx.doi.org/10.1016/j.jsv.2015.03.038
0022-460X/

Brincker et al. [1] proposed a frequency domain method for modal identification of output-only systems. Caicedo et al. [2] applied natural excitation technique and eigensystem realization algorithm on simulated data generated with the popular IASC-ASCE benchmark problem. Ibrahim [3] proposed the random decrement technique for modal identification. There are many other studies dealing with modal identification based damage detection. However, to save space, those are not listed here. On the other hand, feature-based techniques are also getting tremendous attention since the last decade by virtue of their statistical significance and efficiency in damage detection. Sohn and Farrar [4] applied statistical pattern recognition paradigm in structural health monitoring. Cheung et al. [5] experimentally validated the statistical pattern recognition method for damage detection with field data. Anderson et al. [6] have used spatial maps of frequency domain features represented using Gaussian process for dynamic analysis of composite plate. The following literature review will be limited to the feature-based techniques only.

Wandji [7] suggested a nonparametric goodness-of-fit test on parametric autoregressive (AR) model to distinguish between two different sets of data. Worden et al. [8] performed an outlier analysis with discordancy test on a spring–mass–dashpot system for damage detection. Kar and Mohanty [9] used Kolmogorov–Smirnov (KS) test parameters in fault diagnosis of ball bearing. Mattson and Pandit [10] studied the applicability of statistical moments of AR model residual error in damage localization and achieved varying levels of success on a damage simulation test-bed depicting the statistical importance of AR model residual error. Kar and Mohanty [11] also performed motor current signature analysis for multistage gearbox condition monitoring using empirical cumulative distribution. Autoregressive moving average model with exogenous input along with statistical process control are applied by Da Silva et al. [12] on smart structures using simulations and experimental studies. Using multiple ambient excitation on a five-storey building model, Zheng and Mita [13] used the Itakura and the cepstral distances [14] based on AR model for damage localization and quantification. An insight on the usage of applying goodness-of-fit test (Bickel–Rosenblatt test [15]) on AR model residuals was provided by Na [16].

A time domain damage diagnosis algorithm using acceleration response has been illustrated by Gao and Lu [17] showing the strength of residual generation approach in damage detection. Wang and Makis [18] identified KS test parameters on gear shaft fault diagnosis as progressive damage indicators. Dong et al. [19] proposed damage features based on empirical mode decomposition and autoregressive moving average model and also verified their applicability on real structures. Bernal et al. [20] considered the residual error of autoregressive model with exogenous input (ARX model) as a reliable damage detection parameter and validated experimentally. Mosavi et al. [21] proposed damage indices based on AR model coefficients and Mahalanobis distance to detect different severity of damage on steel bridge girder from ambient vibration response. For gearbox damage detection, Zhan and Mechefske [22] used modified AR model coefficients and residual errors with KS test on a simulated model. Later, the usefulness of this methodology has also been verified with experimental evidences [23]. Roy and Ray-Chaudhuri [24] explored the performance of ARX model in the presence of parametric uncertainty in damage localization of an output-only spring–mass–dashpot system with varying levels of damping.

It is clear from the previous discussion that various feature-based techniques have been proposed for damage detection and localization. It is also found that these techniques perform with varying levels of success for different structures and different damage scenarios. In this study, a set of four damage sensitive features (DSFs) are proposed based on ARX model parameters. A mathematical formulation has been derived in this study to establish the relation of these DSFs with structural damage. Subsequently, a numerical illustration has been carried out using a shear building and a steel moment-resisting frame (SMRF) to show the efficiency of these DSFs.

2. Description of ARX model

2.1. General description

Autoregressive model is used popularly to predict future possible data of a signal based on the previous data. The governing equation for the AR model is expressed in the following form:

$$\{y(t)\} = \sum_{i=1}^{g} [A_i]\{y(t-i)\} + \{e(t)\} \tag{1}$$

where $[A_i]$ is the ith coefficient of the model, $\{y(t)\}$ the signal to be predicted, $\{e(t)\}$ the residual error of the model, g the order of the model i.e., the number of previous data to be considered to forecast future data. The coefficients of the model can be calculated by Yule–Walker method [25], the oldest one among a few popular commonly used techniques such as Yule–Walker, Burger and Least Square [26].

In this study, another form of the AR model with exogenous input (ARX model) has been adopted for damage localization. A simplified form of ARX model can be expressed as follows:

$$[A]\{y(t)\} = [B]\{u(t)\} + \{e(t)\} \tag{2}$$

where $\{u(t)\}$ is the exogenous input and $[B]$ is the corresponding coefficient matrix. The reason behind choosing this ARX model instead of the standard AR model is that the coefficients of the ARX model have a direct correlation with the structural stiffness. Such a correlation is however not established for the standard AR model. Let us consider the undamped vibration of an n-degree-of-freedom (dof) shear building as shown in Fig. 1. The equations of motion for this system take the

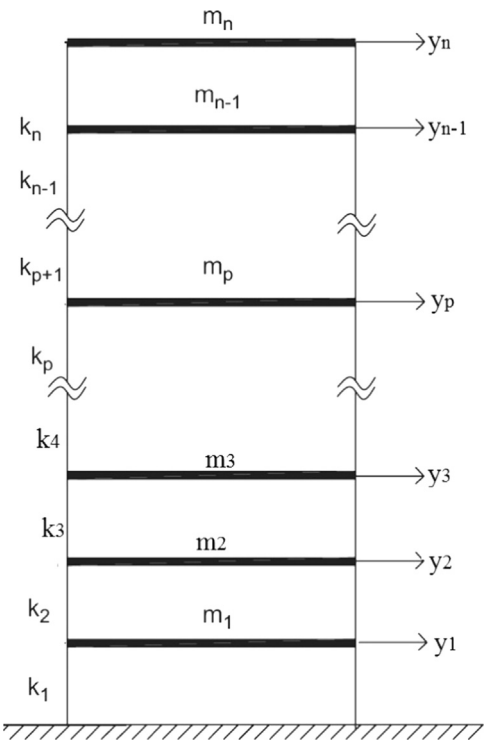

Fig. 1. Schematic diagram of *n*-dof shear building.

following form:

$$[M_0]\{\ddot{y}(t)\}+[K_0]\{y(t)\}=[L_0]\{u(t)\} \tag{3}$$

where $\{y(t)\}$ is a vector of dimension n; $[M_0]$ and $[K_0]$ are mass and stiffness matrices of dimension $n\times n$, respectively; $[L_0]$ is the input coefficient or influence matrix with dimension $n\times m$. Eq. (3) can be re-written as

$$\{\ddot{y}(t)\}+[K]\{y(t)\}=[L]\{u(t)\} \tag{4}$$

where $[K]=[M_0]^{-1}[K_0]$ and $[L]=[M_0]^{-1}[L_0]$. Note that the mass normalized stiffness $[K]$ can be expressed as $[\Phi]^T[\Lambda][\Phi]$, where $[\Phi]$ and $[\Lambda]$ are the mode shape matrix and eigenvalue matrix, respectively. In terms of ARX model with order ARX (a,b), the governing equation may be written as

$$\{\hat{y}(t)\}=\sum_{i=1}^{a}[A_i]\{y(t-i)\}+\sum_{j=1}^{b}[B_j]\{u(t-j+1)\} \tag{5}$$

where $\{\hat{y}(t)\}$ is the predicted signal; $[A_i]$ and $[B_j]$ are the model coefficients. Using two previous data points of the output and three data points of the input (i.e., using a model order ARX(2,3)), Lu and Gao [27] have estimated the coefficients of ARX model as $[A_1]=2\cos([K]^{1/2}\Delta t)$, $[A_2]=-[I]$, $[B_1]=[L]$, $[B_2]=-[\Phi]\left[[I]+\cos([\Lambda]^{1/2}\Delta t)\right][\Phi]^T[L]$ and, $[B_3]=[\Phi]\cos([\Lambda]^{1/2}\Delta t)[\Phi]^T[L]$ with Δt being the sampling period of the series and $[I]$ denoting the identity matrix. Based on their study [27], a model of order ARX(2,3) has been used in this work unless otherwise mentioned.

2.2. ARX model coefficients

In this section, the expression for difference in ARX model coefficients is formulated. From the expression of $[A_1]$, it is evident that the first coefficient of ARX model (i.e., $[A_1]$) is governed by the structural properties such as mass and stiffness of a system. Hence, any damage in the system will lead to a change in $[A_1]$. Further, $[A_1]$ can be expanded in series as follows:

$$[A_1]=2\cos\left([K]^{1/2}\Delta t\right) \tag{6a}$$

$$[A_1]=2[I]-\frac{2}{2!}[K]\Delta t^2+\frac{2}{4!}[K]^2\Delta t^4-\frac{2}{6!}[K]^3\Delta t^6+\cdots\infty \tag{6b}$$

Now, if a system undergoes some damage, the first ARX model coefficient corresponding to the undamaged and damaged states can be noted as $[A_{1u}]$ and $[A_{1d}]$, respectively. The difference between $[A_{1u}]$ and $[A_{1d}]$, i.e., $[\Delta A_1]=[A_{1u}]-[A_{1d}]$ can

therefore be written as

$$[\Delta A_1] = -\frac{2}{2!}([K_u]-[K_d])\Delta t^2 + \frac{2}{4!}([K_u]^2-[K_d]^2)\Delta t^4 - \frac{2}{6!}([K_u]^3-[K_d]^3)\Delta t^6 + \cdots\infty \tag{7a}$$

$$[\Delta A_1] = \sum_{r=1}^{\infty}(-1)^r\frac{2}{(2r)!}([K_u]^r-[K_d]^r)\Delta t^{2r} \tag{7b}$$

Now, let us consider that the damage took place at the pth storey level of the building, which can be simulated as a stiffness degradation of that floor by an amount of δk_p from its original stiffness, k_p. The modified stiffness matrix of the damaged structure takes the following form:

$$[K_d] = \begin{bmatrix} k_1+k_2 & -k_2 & 0 & \cdots & \cdots & \cdots & 0 \\ -k_2 & k_2+k_3 & -k_3 & 0 & \cdots & \cdots & 0 \\ 0 & \cdots & \cdots & \cdots & 0 & \cdots & 0 \\ 0 & 0 & \cdots & k_{p-1}+(k_p-\delta k_p) & -(k_p-\delta k_p) & 0 & 0 \\ 0 & \cdots & 0 & -(k_p-\delta k_p) & (k_p-\delta k_p)+k_{p+1} & \cdots & 0 \\ 0 & \cdots & \cdots & 0 & \cdots & \cdots & \cdots \\ 0 & \cdots & \cdots & 0 & \cdots & \cdots & k_n \end{bmatrix}_{n\times n} \tag{8}$$

The damaged stiffness $[K_d]$ can be alternatively expressed as $[K_d]=[K_u]+[\Delta K_p]$ with $[\Delta K_p]=[I_p]\delta k_p$ and

$$[I_p] = \begin{bmatrix} 0 & 0 & 0 & \cdots & \cdots & \cdots & 0 \\ 0 & 0 & 0 & 0 & \cdots & \cdots & 0 \\ 0 & \cdots & \cdots & \cdots & 0 & \cdots & 0 \\ 0 & 0 & \cdots & -1 & 1 & 0 & 0 \\ 0 & \cdots & 0 & 1 & -1 & \cdots & 0 \\ 0 & \cdots & \cdots & 0 & \cdots & \cdots & 0 \\ 0 & \cdots & \cdots & 0 & \cdots & 0 & 0 \end{bmatrix}_{n\times n} \tag{9}$$

Utilizing the expression of $[K_d]$ and on simplification, the term $([K_d]^r-[K_u]^r)$ of Eq. (7) can be expressed as follows:

$$[K_d]^r-[K_u]^r = \sum_{s=1}^{\infty}{}^rC_s([K_u]^{-1}[I_p])^s[K_u]^s(\delta k_p)^s \tag{10}$$

where ${}^rC_s$ implies the usual binomial coefficient ($=r!/s!(r-s)!$). Combining Eqs. (7) and (10), one can write

$$[\Delta A_1] = -\sum_{r=1}^{\infty}(-1)^r\frac{2}{(2r)!}\sum_{s=1}^{\infty}{}^rC_s([K_u]^{-1}[I_p])^s[K_u]^s(\delta k_p)^s\Delta t^{2r} \tag{11}$$

2.3. Elimination of excitation vector

For a structure undergoing ambient vibration, the input excitation is not typically available. Thus, to implement the ARX model-based approach as derived here (in case of structure undergoing ambient vibration), the excitation vector $\{u(t)\}$ needs to be eliminated from the formulation. Following the formulation given by Lu and Gao [27], this can be achieved. Considering model order of ARX(2,3) Eq. (5) can be rewritten as follows:

$$\{y(t)\} = [A_1]\{y(t-1)\}+[A_2]\{y(t-2)\}+[B_1]\{u(t)\}+[B_2]\{u(t-1)\}+[B_3]\{u(t-2)\}+\{e(t)\} \tag{12}$$

where the output vector $\{y(t)\}=\{y_1(t)\ y_2(t)\ \ldots\ y_n(t)\}^T$ and $\{e(t)\}$ is the residual error vector. Consider the system to be a single-input–multiple-output one, where input is acting only at the 1st dof for damage at any intermediate storey, i.e., $\{u(t)\}=\{u_1(t)\ 0\ \ldots\ 0\}^T$. It may be noted that any dof could be considered as reference point; however, in this case, the 1st dof is chosen as the input. Hence, Eq. (12) can be rewritten as follows:

$$\{y(t)\} = [A_1]\{y(t-1)\}+[A_2]\{y(t-2)\}+[B_1]\{u_1(t)\ 0\ \ldots\ 0\}^T+[B_2]\{u_1(t-1)\ 0\ \ldots\ 0\}^T+[B_3]\{u_1(t-2)\ 0\ \ldots\ 0\}^T+\{e(t)\} \tag{13}$$

On simplifying Eq. (13), the following expression can be obtained:

$$\{y(t)\} = [A_1]\{y(t-1)\}+[A_2]\{y(t-2)\}+\{B_1(c_1)\}u_1(t)+\{B_2(c_1)\}u_1(t-1)+\{B_3(c_3)\}u_1(t-2)+\{e(t)\} \tag{14}$$

where $\{B_1(c_1)\}$, $\{B_2(c_1)\}$ and $\{B_3(c_1)\}$ are the column vectors corresponding to the first column of the matrices $[B_1]$, $[B_2]$ and $[B_3]$, respectively. Now, from Eq. (12), $y_1(t)$ can be expressed as

$$y_1(t) = [A_1(r_1)]\{y(t-1)\}+[A_2(r_1)]\{y(t-2)\}+B_1(r_1,c_1)u_1(t)+B_2(r_1,c_1)u_1(t-1)+B_3(r_1,c_1)u_1(t-2)+e_1(t) \tag{15}$$

where $[A_1(r_1)]$ and $[A_2(r_1)]$ are the row matrices corresponding to the first row of the matrices $[A_1]$ and $[A_2]$, respectively. Also, $B_1(r_1,c_1)$, $B_2(r_1,c_1)$ and $B_3(r_1,c_1)$ are the elements corresponding to first row and first column of the matrices $[B_1]$, $[B_2]$ and $[B_3]$, respectively. For $B_1(r_1,c_1)\neq 0$,

$$u_1(t)=\frac{1}{B_1(r_1,c_1)}\left[y_1(t)-[A_1(r_1)]\{y(t-1)\}-[A_2(r_1)]\{y(t-2)\}\right] -\frac{1}{B_1(r_1,c_1)}[B_2(r_1,c_1)u_1(t-1)+B_3(r_1,c_1)u_1(t-2)+e_1(t)] \tag{16}$$

Now without its 1st row, $\{y(t)\}$ is expressed as $\{y^*(t)\}$, i.e., $\{y^*(t)\}=\{y_2(t)\ y_3(t)\ \dots\ y_n(t)\}^T$. Thus, Eq. (14) can be expressed as follows:

$$\{y^*(t)\}=[A_1^*]\{y(t-1)\}+[A_2^*]\{y(t-2)\} +\{B_1^*(c_1)\}u_1(t)+\{B_2^*(c_1)\}u_1(t-1)+\{B_3^*(c_1)\}u_1(t-2)+\{e^*(t)\} \tag{17}$$

where $[A_1^*]$ and $[A_2^*]$ are the matrices without the 1st rows of $[A_1]$ and $[A_2]$, respectively; $\{B_1^*(c_1)\}$, $\{B_2^*(c_1)\}$, $\{B_3^*(c_1)\}$ and $\{e^*(t)\}$ are the same as the column vectors $\{B_1(c_1)\}$, $\{B_2(c_1)\}$, $\{B_3(c_1)\}$ and $\{e(t)\}$, respectively, except without their 1st elements. Now substituting the expression of $u_1(t)$ from Eq. (16) into Eq. (17), the following expression can be obtained.

$$\begin{aligned}\{y^*(t)\}=&\left([A_1^*]-\frac{1}{B_1(r_1,c_1)}\{B_1^*(c_1)\}[A_1(r_1)]\right)\{y(t-1)\}\\&+\left([A_2^*]-\frac{1}{B_1(r_1,c_1)}\{B_1^*(c_1)\}[A_2(r_1)]\right)\{y(t-2)\}\\&+\frac{1}{B_1(r_1,c_1)}\{B_1^*(c_1)\}y_1(t)+\left(\{B_2^*(c_1)\}-\frac{B_2(r_1,c_1)}{B_1(r_1,c_1)}\{B_1^*(c_1)\}\right)u_1(t-1)\\&+\left(\{B_3^*(c_1)\}-\frac{B_3(r_1,c_1)}{B_1(r_1,c_1)}\{B_1^*(c_1)\}\right)u_1(t-2)+\left[\{e^*(t)\}-\frac{1}{B_1(r_1,c_1)}\{B_1^*(c_1)\}e_1(t)\right]\end{aligned} \tag{18}$$

For very large sampling frequency of the output data, i.e., for very small values of Δt, $[B_1]=L$, $[B_2]=-2L$, and $[B_3]=L$. Therefore, the coefficients of $u_1(t-1)$ and $u_1(t-2)$ vanish i.e., $\left(\{B_2^*(c_1)\}-(B_2(r_1,c_1)/B_1(r_1,c_1)\{B_1^*(c_1)\}\right)=0$ and $\left(\{B_3^*(c_1)\}-(B_3(r_1,c_1)/B_1(r_1,c_1))\{B_1^*(c_1)\}\right)=0$. Therefore, Eq. (18) can be expressed as follows:

$$\{y^*(t)\}=[\bar{A}_1^*]\{y(t-1)\}+[\bar{A}_2^*]\{y(t-2)\}+[\bar{B}_1^*]\{y_1(t)\}+\{\bar{e}^*(t)\} \tag{19}$$

where the coefficient matrices $\bar{B}_1^*=(1/B_1(r_1,c_1))\{B_1^*(c_1)\}$, $\bar{A}_1^*=\left([A_1^*]-(1/B_1(r_1,c_1))\{B_1^*(c_1)\}[A_1(r_1)]\right)$ and $\bar{A}_2^*=\left([A_2^*]-(1/B_1(r_1,c_1))\{B_1^*(c_1)\}[A_2(r_1)]\right)$. Note that $[\bar{A}_1^*]$ is a matrix with dimension $(n-1)\times n$. Consider $[\bar{A}_1^*]=\left[\{\bar{A}_1^*(c_1)\}\ [\bar{A}_1^{*\dagger}]\right]$, where $\{\bar{A}_1^*(c_1)\}$ is a vector corresponding to the first column of $[\bar{A}_1^*]$. Here, $\{\bar{A}_1^*(c_1)\}$ and $[\bar{A}_1^{*\dagger}]$ are with dimensions $(n-1)\times 1$ and $(n-1)\times(n-1)$, respectively. In the same manner, $[A_2^*]$ can also be expressed. Now, $\{y^*(t)\}$ can be written as

$$\{y^*(t)\}=\left(\{\bar{A}_1^*(c_1)\}\ [\bar{A}_1^{*\dagger}]\right)\begin{pmatrix}y_1(t-1)\\ \{y^*(t-1)\}\end{pmatrix}+\left(\{\bar{A}_2^*(c_1)\}\ [\bar{A}_2^{*\dagger}]\right)\begin{pmatrix}y_1(t-2)\\ \{y^*(t-2)\}\end{pmatrix}+\{\bar{B}_1^*\}y_1(t)+\{\bar{e}^*(t)\} \tag{20}$$

where $\{y^*(t-1)\}$ and $\{y^*(t-2)\}$ denote the vectors $\{y(t-1)\}$ and $\{y(t-2)\}$, respectively, except without their first rows. Hence, Eq. (20) can be expressed in the following form:

$$\{y^*(t)\}=[\bar{A}_1^{*\dagger}]\{y^*(t-1)\}+[\bar{A}_2^{*\dagger}]\{y^*(t-2)\}+\{\bar{B}_1^*\}y_1(t)+\{\bar{A}_1^*(c_1)\}y_1(t-1)+\{\bar{A}_2^*(c_1)\}y_1(t-2)+\{\bar{e}^*(t)\} \tag{21}$$

One can note that Eq. (21) is analogous with Eq. (14) except that the input $u_1(t)$ is replaced by the first element of output $y_1(t)$ and the coefficient matrices are different. Thus, in the absence of $u_1(t)$, one can use $y_1(t)$ in the same way as in Eq. (14) to obtain remaining $\{y^*(t)\}$ (i.e., for the other dofs). This concept has been employed in the following numerical analysis.

2.4. ARX model residual error

The deviation of data predicted by the ARX model from its actual data is the residual error, which is ideally a Gaussian process for a stationary signal [28]. Damage at a particular floor alters the model coefficients by changing mainly the four elements of the first coefficient, as shown in the previous section. Using Eq. (5), the residual error for both undamaged and damaged cases can be estimated from the following equations:

$$\{e_u(t)\}=\{y_u(t)\}-\{\hat{y}_u(t)\} \tag{22a}$$

$$\{e_d(t)\}=\{y_d(t)\}-\{\hat{y}_u(t)\} \tag{22b}$$

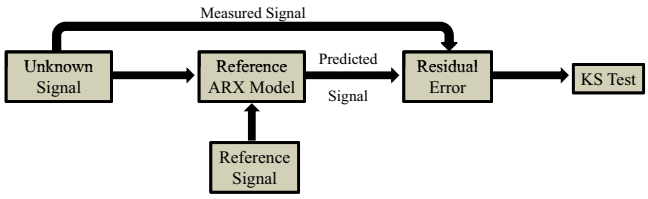

Fig. 2. The proposed algorithm for KS test statistical distance.

where $\{y_u(t)\}$ and $\{y_d(t)\}$ are the undamaged and damaged responses from the structure, respectively, and $\{\hat{y}_u(t)\}$ is the signal predicted from the undamaged (reference) state, which can be expressed as follows:

$$\{\hat{y}_u(t)\} = \left(\sum_{i=1}^{2} [A_i]\{y(t-i)\} + \sum_{j=1}^{3} [B_j]\{u(t-j)\} \right) \tag{23}$$

As the input excitation to the system may not be available, any output response can be considered as the exogenous input and remaining as the output of the system in the framework of ARX model [27]. The algorithm in the form of a flowchart is shown in Fig. 2. As one of the output response of the system is assumed as the (dummy) input, the residual error of this particular dof cannot be determined. Also from Fig. 2, one can observe that the residual error corresponding to the unknown signal is estimated from the unknown signal applied to the reference ARX model.

3. Damage sensitive features

3.1. Difference in AR model coefficients (DARC)

The analytical expression of difference in first ARX model coefficients is given in Eq. (11). Now, for small value of storey stiffness reduction at the pth level (δk_p), the higher order terms of δk_p can be neglected i.e., for $s=1$ only δk_p is retained leading Eq. (11) into the following form:

$$[\Delta A_1] = -\sum_{r=1}^{\infty} (-1)^r \frac{2}{(2r)!} r [K_u]^{-1} [I_p] [K_u] \delta k_p \Delta t^{2r} \tag{24}$$

Again, for small time step, Δt^{2r} turns to be negligible as r increases. Therefore, for $r=1$, one can write

$$[\Delta A_1] = [K_u]^{-1} [I_p] [K_u] \Delta t^2 \delta k_p \tag{25}$$

Eq. (25) shows that $[\Delta A_1]$ is directly proportional to the storey stiffness degradation and only affects the non-zero term of $[I_p]$. So the elements of $[\Delta A_1]$ matrix corresponding to the positions $(p-1,p-1),(p-1,p),(p,p-1)$, and (p,p) attain large values (proportional to the intensity of damage) compared to the rest of the elements of this matrix. Therefore, the damage can be localized and quantified by identifying these four high-valued elements in the matrix, $[\Delta A_1]$. Therefore, the difference in the first ARX model coefficients (henceforth will be termed as DARC) can be used as a DSF. As the first dof is considered as the input of the structure, the first coefficient of ARX model (as shown in Eq. (21)) does not contain the first row and first column corresponding to the first dof. Hence, $[\Delta A_1]$ is a matrix with dimension of $(n-1)\times(n-1)$.

3.2. Kolmogorov–Smirnov statistical distance (KSTD)

Statistical inferences such as standard deviation, skewness, and kurtosis of autoregressive model residual error carry vital information of the data. Since it is difficult to obtain the input excitation data of a structure under operating condition, it is often assumed that the input excitation to be a zero mean Gaussian white noise. Hence, the system responses are expected to follow a Gaussian distribution [29]. Thus, ARX model can be used for time series modelling of the data. From Eq. (22), it is clear that the residual error of the damaged data is different than that of the undamaged one.

There are many available statistical hypothesis tests to compare two different data sets. They are broadly classified into two categories: parametric test and nonparametric test. Before applying any parametric test, a maximum likelihood estimate of the considered data set is to be performed leading to a prior assumption of the data to follow a particular distribution. Hence F-test, student's t-test, χ^2 test, etc. cannot be applied in the present study. KS test (a nonparametric test) takes empirical cumulative distribution function (ECDF) to determine the maximum statistical distance. This is further used to judge whether two different data sets are drawn from same underlying distribution for a particular significance level. In KS test, no prior assumption towards the distribution pattern is needed and a graphical visualization of ECDF may provide some idea about distribution of the data. Because of these advantages, KS test is considered as one of the most preferred statistical signal processing tool in time domain signal analysis [9]. In this paper, two-sample KS test is adopted to check the comparability between the residual errors of the undamaged and damaged data sets [11].

In this study, an ARX model is developed with the known reference signal and the residual error is calculated for the undamaged case. Thereafter, for a damaged case, the residual error is calculated utilizing the deviation of the damaged response data from the reference ARX model data. The similarity between the two distinguished data sets of residual error (undamaged and damaged) is signified through KS test.

Let the ARX model residual error vector from the undamaged and damaged data sets be $\{e_u(t)\}$ and $\{e_d(t)\}$, respectively. Here, the test statistics play a major role in this nonparametric hypothesis test to decide whether null hypothesis $\mathbb{H}_0$ is to be rejected for a given confidence interval. Let the ECDF of undamaged and damaged residual errors are $\{F_u(t)\}$ and $\{F_d(t)\}$, respectively. Consequently, the hypothesis and test statistics take the following form:

$$\mathbb{H} = \text{hypothesis} = \begin{cases} 1, & e_u \neq e_d \\ 0, & e_u \equiv e_d \end{cases} \tag{26a}$$

$$\text{KSTD} = \text{KS test statistical distance} = |\{F_u(t)\} - \{F_d(t)\}|_{\max} \tag{26b}$$

where

$$\{F(t)\} = \text{empirical distribution function} = \frac{1}{n}\sum_{i=1}^{n} I(t_i \leq t) \tag{27a}$$

$$I = \text{indicator of the event} = \begin{cases} 1, & t_i \leq t \\ 0 & \text{otherwise} \end{cases} \tag{27b}$$

Further, this statistical distance, henceforth termed as KSTD is established to construct a damage sensitive feature.

3.3. Confidence interval to peak-pdf ratio (CIPR)

In Eq. (22b), the residual error corresponding to the damaged structural response is estimated as the difference between the actual damaged response and the predicted undamaged response (provided in Eq. (23)). On the other hand, the residual error corresponding to the undamaged state is the difference between the actual undamaged response and the undamaged predicted response, which is negligible by virtue of its evaluation. Now, from Eqs. (22) and (23), the residual error for the damaged system can be expressed as

$$\{e_d(t)\} = \{y_d(t)\} - \left(\sum_{i=1}^{2}[A_i]\{y(t-i)\} + \sum_{j=1}^{3}[B_j]\{u(t-j)\}\right) \tag{28}$$

One can infer from Eq. (28) that a damage at any intermediate storey affects only four elements $[A_i]$ (see Eqs. (9) and (11)). Therefore, it is imperative from the expression of $[A_i]$ that $\{e_u(t)\}$ differs more from $\{e_d(t)\}$ at the two dofs adjacent to the damaged stiffness.

As the structure is assumed to be excited with a band-limited white noise, the structural response would follow a Gaussian distribution. Now, the ARX model is constructed using this structural response and therefore, the residual error from the ARX model will follow a Gaussian distribution [28]. Fig. 3 shows schematically the probability density function (pdf) of the residual errors corresponding to the undamaged as well as damaged state for a given damage location. From Fig. 3, one can observe that the pdf of residual error corresponding to damaged dof is comparatively more dispersed and the

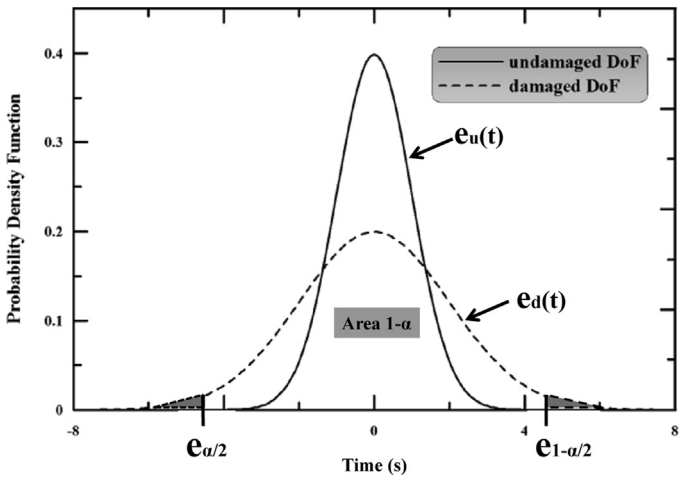

Fig. 3. Schematic diagram of the pdf of residual error.

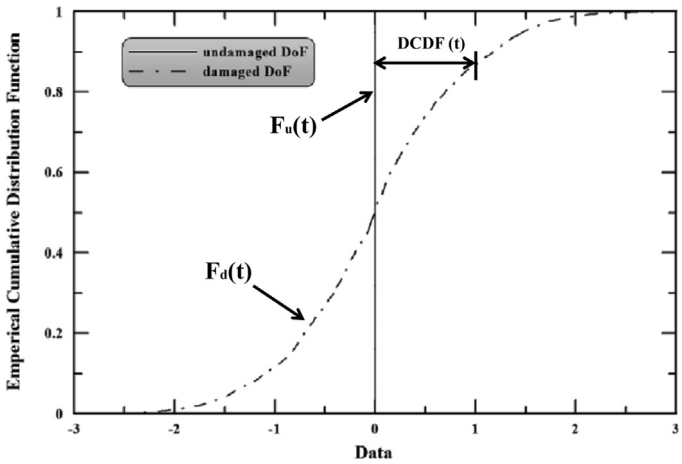

Fig. 4. Schematic diagram of the ECDF of residual error.

maximum value of the pdf is less than that of the undamaged dof. Both of these measures can be utilized in damage localization. As the residual error corresponding to undamaged state is negligible, its pdf attains a Dirac delta-type function. Hence, the ratio of any confidence interval to the maximum value of the pdf of $\{e_d(t)\}$ can be considered as a good measure to identify the damage location. The pdf of residual error can be expressed as

$$f_{\text{res}}(e) = \frac{1}{\sqrt{2\pi}\sigma_{\text{res}}} \exp \frac{(e_d(t(-\mu_{\text{res}})^2}{2\sigma_{\text{res}}^2} \tag{29}$$

where μ_{res} and σ_{res}, respectively, are the mean and standard deviation of the residual error. Considering a significance level of α, a feature can be proposed as the ratio of the confidence interval to peak pdf as shown in Fig. 3. The confidence interval to peak pdf ratio (CIPR) can be mathematically expressed as

$$\text{CIPR} = \frac{e_{d(1-\alpha/2)} - e_{d(\alpha/2)}}{f_{\max}} \tag{30}$$

The significance level can be assumed to be of any reasonable value. In this study, 95 percent confidence interval is adopted to quantify the dispersion of the pdf, i.e., $\alpha = 0.05$. Therefore, the ratio of the 95 percent confidence interval and peak value of the pdf of ARX model residual error corresponding to the damaged signal is proposed as another DSF. As the residual error corresponding to the dummy input (in the framework of ARX model) cannot be calculated, the CIPR of that dof is assumed to be zero in the numerical illustration.

3.4. *Difference in cumulative distribution function (DCDF)*

As described earlier, the residual error of the dofs adjacent to the damage location is different from that of the undamaged ones from statistical point of view. In this section, another statistical parameter, namely, empirical cumulative distribution function (ECDF) is utilized to define a feature sensitive to structural damage location. ECDF (i.e., $\{F(t)\}$), as given in Eq. (27a), is a very useful statistical measure for characterization of any data. This is a step function starting from zero to unity. It estimates the true cumulative distribution of the data following an indicator function, given in Eq. (27b). Now to obtain ECDF, the following steps are to be followed: (i) rearrangement of data in ascending order, (ii) evaluation of event indicator and (iii) plot the empirical cumulative distribution function. In the vicinity of damage location, $\{F_d(t)\}$ deviates more from $\{F_u(t)\}$. Fig. 4 schematically shows the ECDF plot of the residual error for a dof adjacent to a damage location. It depicts that the ECDF of residual error corresponding to any damaged dof deviates from that of the undamaged one. Therefore, the difference in ECDF for all data points will vary considerably in the vicinity of the damaged location and can be used as a damage location indicator. This difference in ECDF (henceforth will be termed as DCDF) will be used as another DSF for damage localization. Although both DCDF and KSTD utilize ECDF as the starting point for evaluation, they are different. In addition, DCDF provides a graphical representation for damage location instead of numerical value as in KSTD.

4. Numerical illustration

In this section, a numerical study is conducted to investigate the performance of the proposed DSFs (i.e., DARC, KSTD, CIPR and DCDF) in damage localization and quantification. For this purpose, a 12-storey shear building and a 12-storey SMRF are considered as shown in Fig. 5. A short description of these buildings and their numerical models are presented followed by the results.

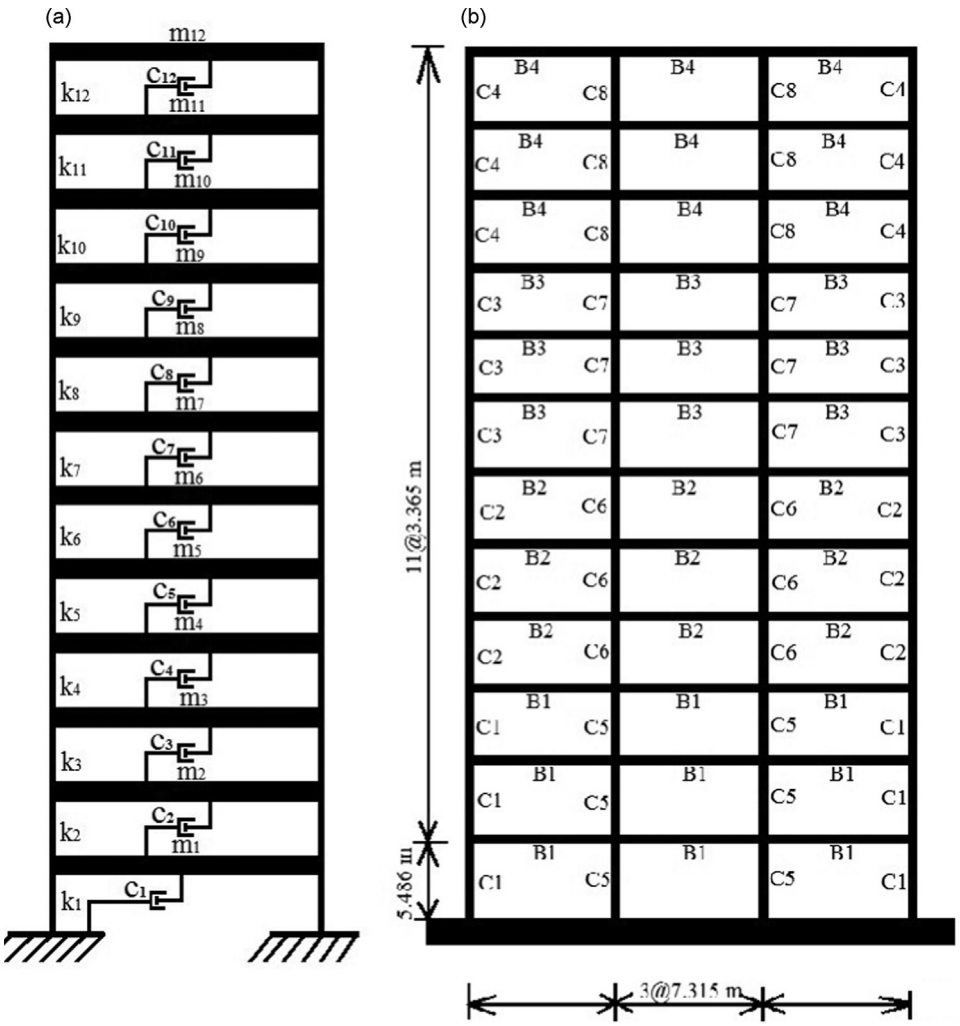

Fig. 5. Numerical models: (a) shear building and (b) steel moment-resisting frame (SMRF).

4.1. Shear building

For the shear building, it is assumed that the system has a uniform nodal mass of $m = 1.0 \times 10^5$ kg and storey stiffness of $k = 2.0 \times 10^8$ N/m. An eigenvalue analysis has been performed and the first three undamped natural periods are determined as $T_1 = 4.3031$ s, $T_2 = 1.4419$ s and $T_3 = 0.8744$ s. An ambient condition is simulated by a zero mean Gaussian white noise base acceleration of standard deviation 0.01g. The shear building is subjected to the aforementioned base excitation and the acceleration responses at different dofs were recorded for 15 min with a sampling rate of 100 Hz. Nigam–Jennings algorithm [30] has been adopted to calculate the response of the structure. In the absence of input information, one of the output responses is assumed as the input in the framework of ARX model. Here, the response of dof 1 is taken as the input to the system while the responses of remaining 11 dofs are considered as output. For the damaged condition, a stiffness degradation of 20 percent is assumed at the 6th storey level.

Figs. 6(a) and 6(b) show sample time histories (duration = 1 s) of the acceleration response of dof 6 for the undamaged and damaged cases, respectively. The predicted responses through ARX model are also plotted in these figures. One can infer from these plots that there is no visible deviation between actual and predicted data for both damaged and undamaged cases. To see how the predicted signal deviates from the actual data, residual error is calculated. The residual errors corresponding to the same location (dof 6) for damaged and undamaged cases are plotted in Figs. 7(a) and 7(b), respectively. To show the nature of variation of residual error in longer time scale for the damaged and undamaged cases, a duration of ten seconds is considered. It can be observed from these figures that (i) the order of magnitude of residual error is more for the damaged case in comparison to the undamaged one and (ii) residual error in case of the undamaged case is dominated by higher frequency content in comparison to the residual error for the damaged case.

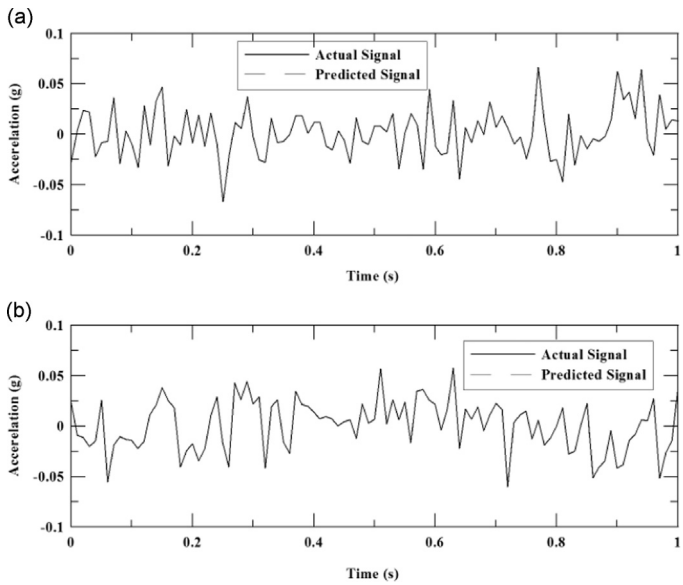

Fig. 6. Sample structural response time history: (a) undamaged state and (b) damaged state.

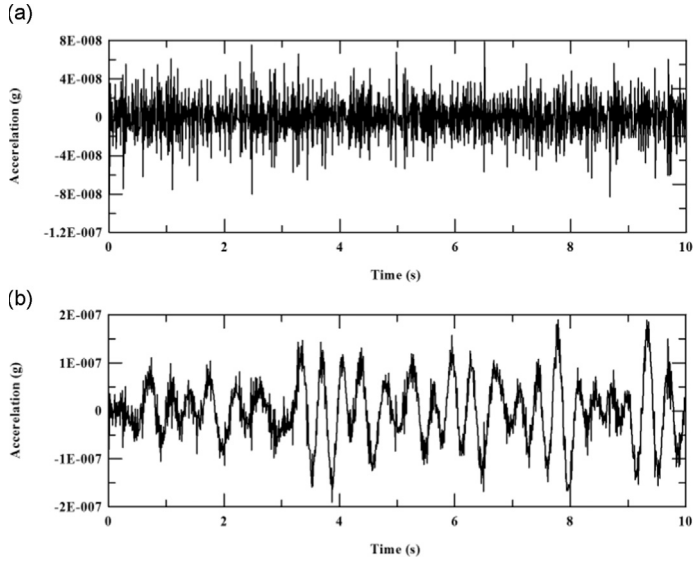

Fig. 7. Sample residual error plot with time: (a) undamaged state and (b) damaged state.

The ARX model coefficients and residual errors are estimated from the ARX model of the undamaged and damaged cases. The damage sensitive features (i.e., DARC, KSTD, CIPR and DCDF) are calculated following the procedure as described in Section 3.

4.1.1. Damage localization

Fig. 8(a) shows a three-dimensional bar plot of the DARC (i.e., difference between the first autoregressive model coefficients corresponding to the undamaged and damaged states). It can be observed from Fig. 8(a) that the DARC shows large values at two diagonal elements (5,5), (6,6) and two off-diagonal elements (5,6), (6,5). This is because the elements of the first ARX model coefficient corresponding to the damage location are proportional to the stiffness of the system, as shown in Eq. (25). Fig. 8(b) is a two-dimensional bar plot of KSTD for each dof normalizing its maximum value to unity. One can observe from the figure that the value of KSTD attains the largest value near the location of damage (i.e., between dof 5 and dof 6 implying the 6th storey level). Fig. 8(c) presents the bar plot of CIPR. It can be noted from the figure that a large value of the ratio occurs near the location of damage. Fig. 8(d) provides a plot of DCDF for different dofs. It is clear from this

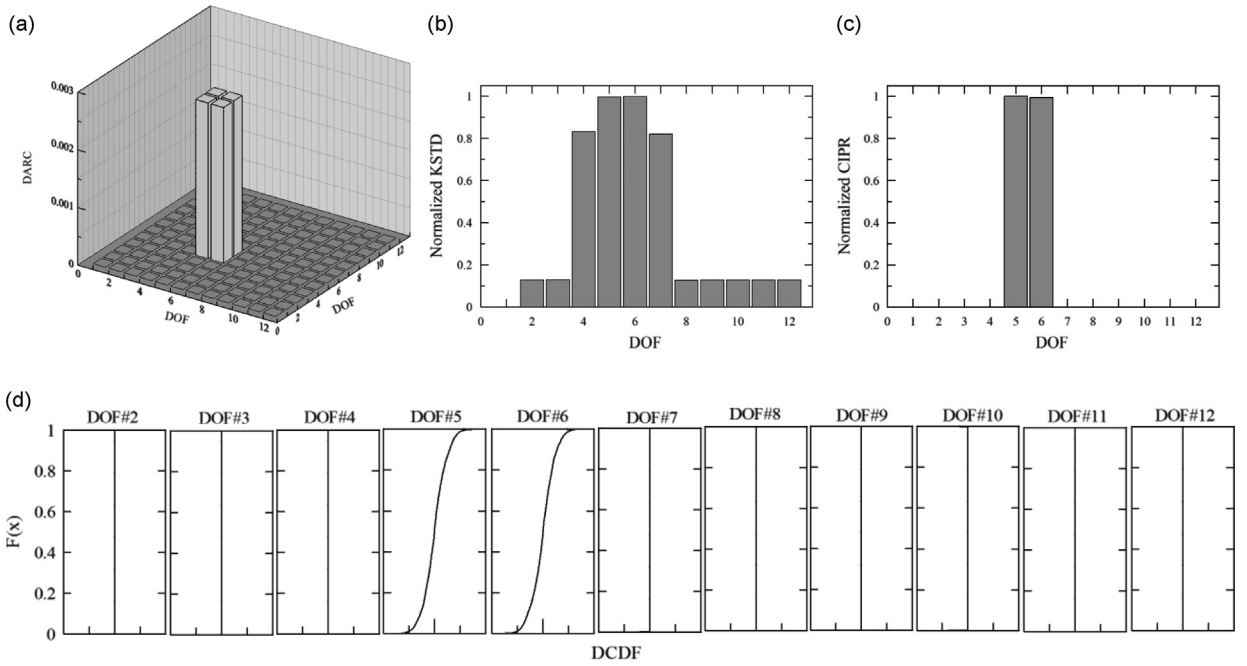

Fig. 8. DSFs of undamped shear building for damage at 6th storey level: (a) DARC, (b) KSTD, (c) CIPR, and (d) DCDF (within -4×10^{-4} to 4×10^{-4}).

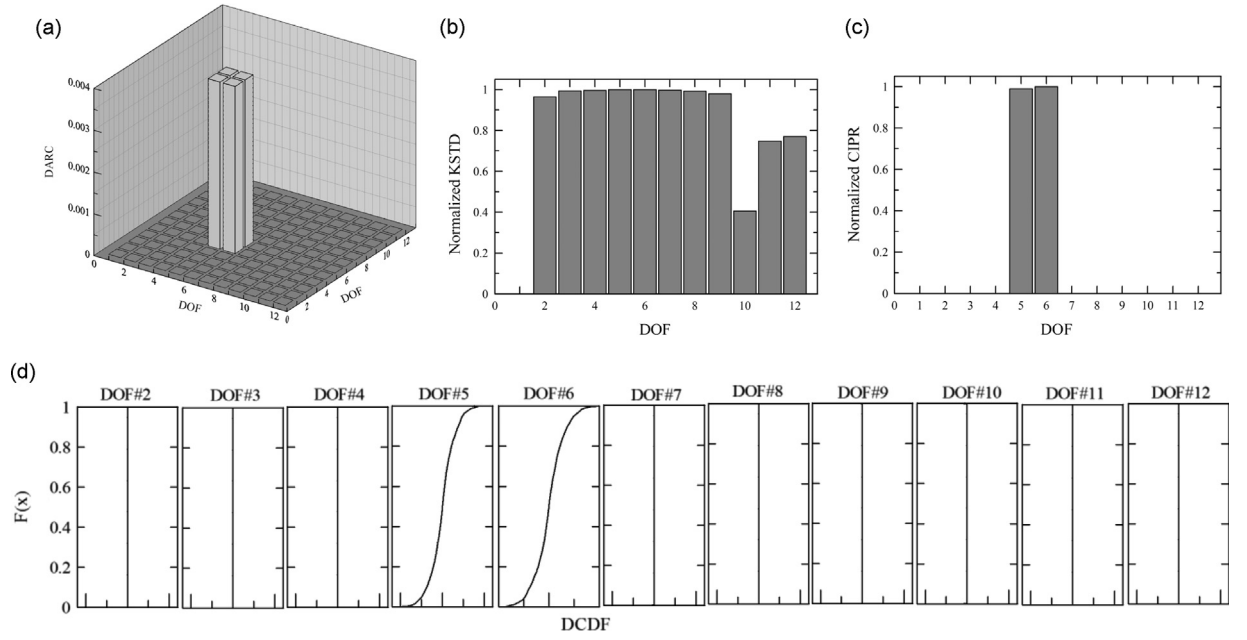

Fig. 9. DSFs of shear building for damage at 6th storey level using ARX model order of five: (a) DARC, (b) KSTD, (c) CIPR, and (d) DCDF (within -12×10^{-4} to 12×10^{-4}).

figure that the damage location is between the 5th and 6th floor levels i.e., at the 6th storey of the system. By comparing Fig. 8(a)–(d), one can notice that all DSFs are highly efficient in accurate localization of damage.

Influence of ARX model order on DSFs: To investigate how the performance of these DSFs varies with ARX model order, the DSFs are evaluated using model order of ARX(5,3) (i.e, keeping the same number of input data points and changing only the number of output data points). Here, the damage location and all other parameters are kept same as considered in Section 4.1.1. Fig. 9(a)–(d) shows the plots of DARC, KSTD, CIPR, and DCDF. It can be observed from these figures that except KSTD (Fig. 9(b)), the other DSFs can successfully localize damage. Further, to ascertain on the performance of KSTD on damage

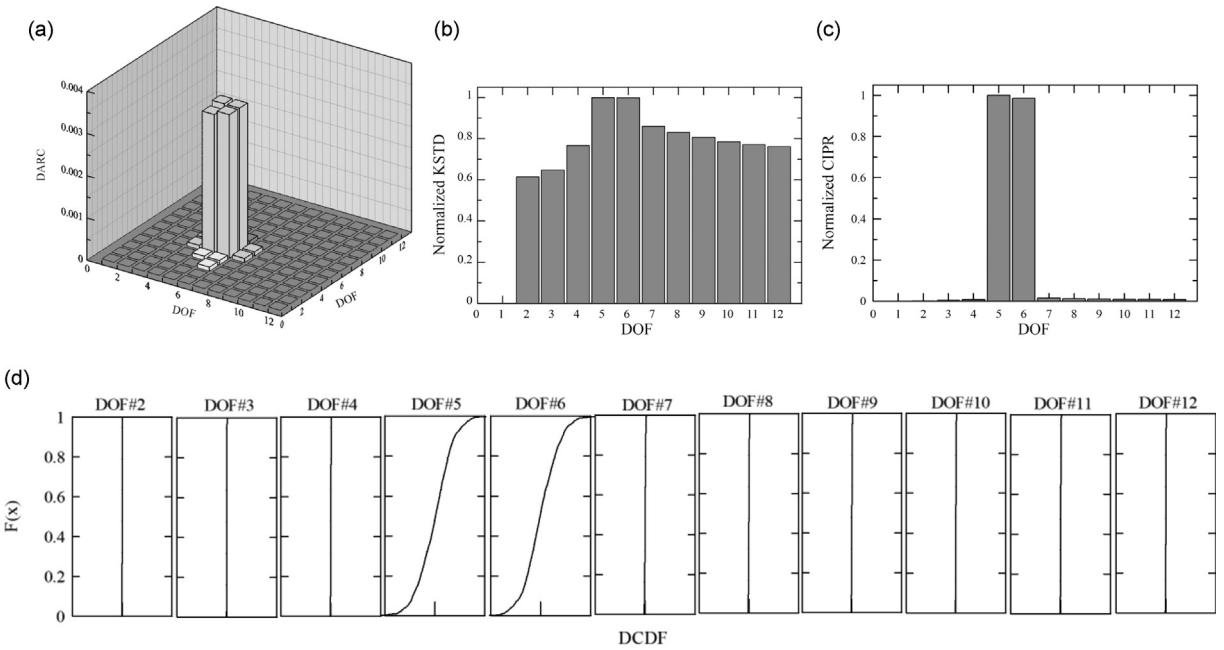

Fig. 10. DSFs of 5% damped shear building for damage at 6th storey level: (a) DARC, (b) KSTD, (c) CIPR, and (d) DCDF (within -5×10^{-5} to 5×10^{-5}).

localization, a study is conducted with varying ARX model order. It is observed that with the increase in model order, the performance of KSTD deteriorates. Therefore, a model of order ARX(2,3) is considered in this study as it is appropriate for estimating all DSFs.

Performance of DSFs in the presence of damping: In order to see the effectiveness of the proposed DSFs in the presence of damping, 5 percent damping has been considered in the shear building. Damage location and all other parameters are considered the same as earlier. Fig. 10(a)–(d) shows the DSFs for this damped case. One can observe from Fig. 10(a), (c) and (d) that DARC, CIPR, and DCDF can successfully locate the damage at the 6th storey level. Although the KSTD value is large for all dofs as shown in Fig. 10(b), the maximum value can be observed at dof 5 and 6, indicating the damaged location. One may however conclude that all other DSFs perform better than KSTD in terms of localizing damage. This is because the way KSTD is evaluated from the ECDF.

4.1.2. *Effect of uncertainties on DSFs*

Structural response measured using sensors may show some fluctuation without any observable alteration in structural parameters. These variations are mainly attributed to the measurement noise and environmental factors that change structural parameters. Usually, the dynamic behaviour of any structural system is governed by two fundamental types of uncertainties [31]: measurement data uncertainty and model parametric uncertainty.

Performance of DSFs in the presence of measurement noise: Noise in the sensor data is inevitable for real measurement conditions. In order to check the effectiveness of the DSFs in handling measurement noise, a 10 percent noise (equivalent to the signal to noise ratio, SNR = 20 dB) is added to the structural response. Fig. 11(a)–(d) shows the plots of DARC, KSTD, CIPR and DCDF. Here, the plots of KSTD (Fig. 11(b)) and CIPR (Fig. 11(c)) show their maximum values around the damage location. However, the plots of DARC (Fig. 11(a)) and DCDF (Fig. 11(d)) indicate false damage locations in addition to the actual damage location. Thus, if four DSFs are used together, damage location can be identified in the presence of measurement noise.

Performance of DSFs in the presence of parametric uncertainties: Most of the existing damage detection methods consider the structural parameters as deterministic. Since, parametric uncertainty renders uncertain response of structures, it may be difficult to identify structural damage in the presence of significant parametric uncertainty. Based on previous studies [32,33], the structural stiffness has been taken as uncertain parameter in this study.

To deal with uncertainty in structural parameters, various approaches have been commonly employed. For example, some common approaches are probability theory [34,35], fuzzy set theory [36], stochastic finite element method [37], interval analysis [38], meta-modelling [39], etc. Among them, the probability theory is the most popular and thus, used in this work to deal with parametric uncertainty. According to Xu et al. [34] and Zhang et al. [35], uncertainty in structural parameters can be expressed in the form of a certain distribution function. In this study, only normal distribution has been considered to model uncertainty in structural stiffness.

The elements of stiffness matrix of the shear building (Fig. 5(a)) are assumed to follow a normal distribution with mean $\mu_k = 2\times10^8$ N/m and coefficient of variation of 5 percent, i.e., standard deviation, $\sigma_k = 0.1\times10^8$ N/m. A 95 percent confidence interval is considered to choose the stiffness value (i.e., within $\mu_k - 1.96\sigma_k = 1.804\times10^8$ N/m and

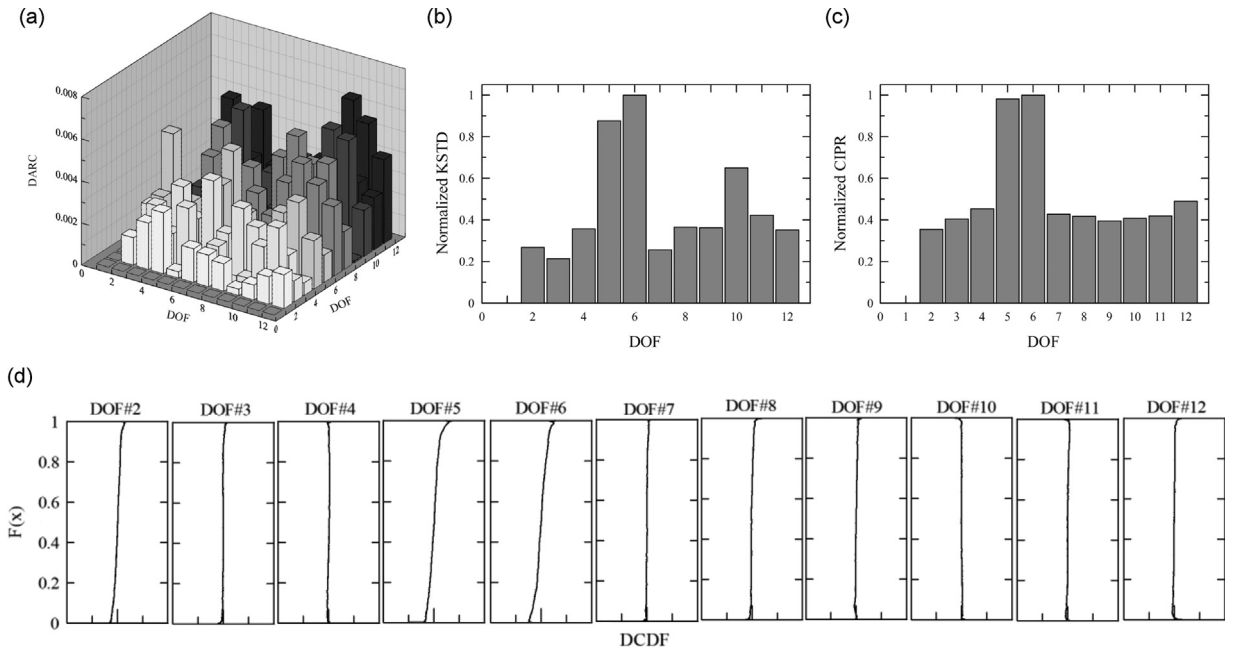

Fig. 11. DSFs of shear building for damage at 6th storey level in the presence of measurement noise: (a) DARC, (b) KSTD, (c) CIPR, and (d) DCDF (within -12×10^{-4} to 12×10^{-4}).

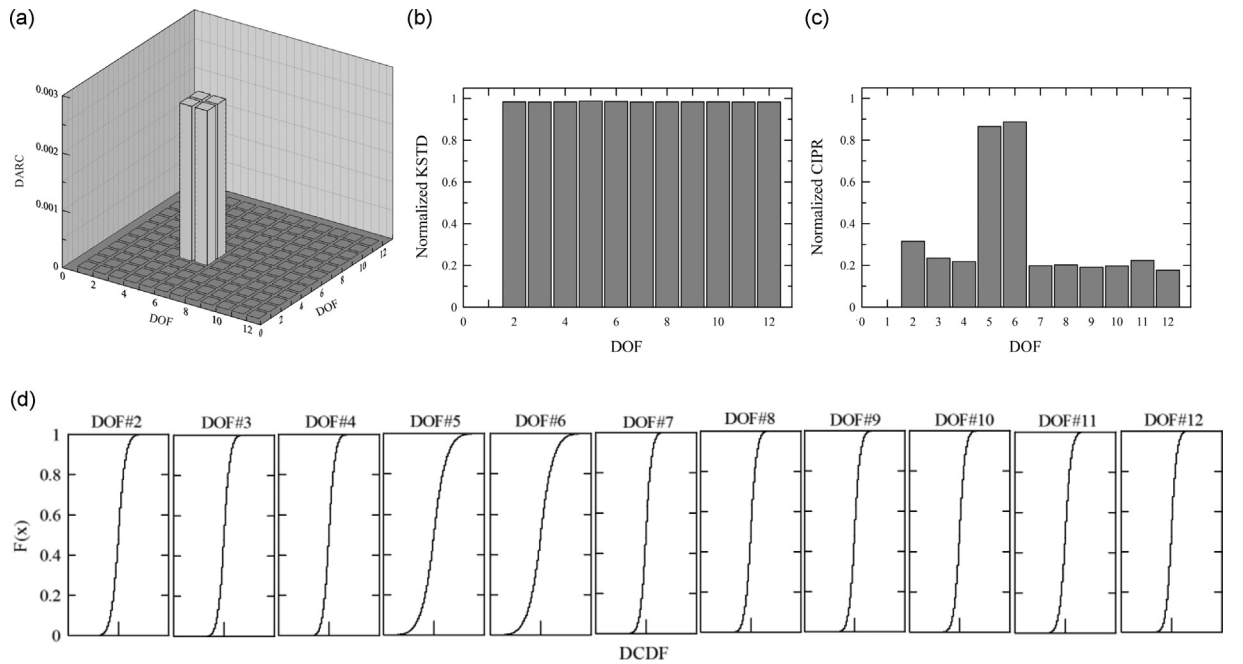

Fig. 12. DSFs of shear building for damage at 6th storey level in the presence of structural parametric uncertainties: (a) DARC, (b) KSTD, (c) CIPR, and (d) DCDF (within -4×10^{-3} to 4×10^{-3}).

$\mu_k+1.96\sigma_k=2.196\times10^8$ N/m), thus eliminating the negative values of storey stiffness. Note, the absolute maximum deviation of any element of stiffness matrix is ±9.8 percent from its deterministic value. Damage location and all other parameters considered here are the same as Section 4.1.1.

In this study, to generate 100 realizations of stiffness matrix considering the uncertainty in structural storey stiffness, Latin hypercube sampling (LHS) technique described by Minasny and McBratney [40] is employed. The simple random sampling (SRS) of the input variables usually requires a large number of realizations to be statistically meaningful. This leads the entire methodology to a computationally cumbersome one. However, the LHS is based on a stratified sampling

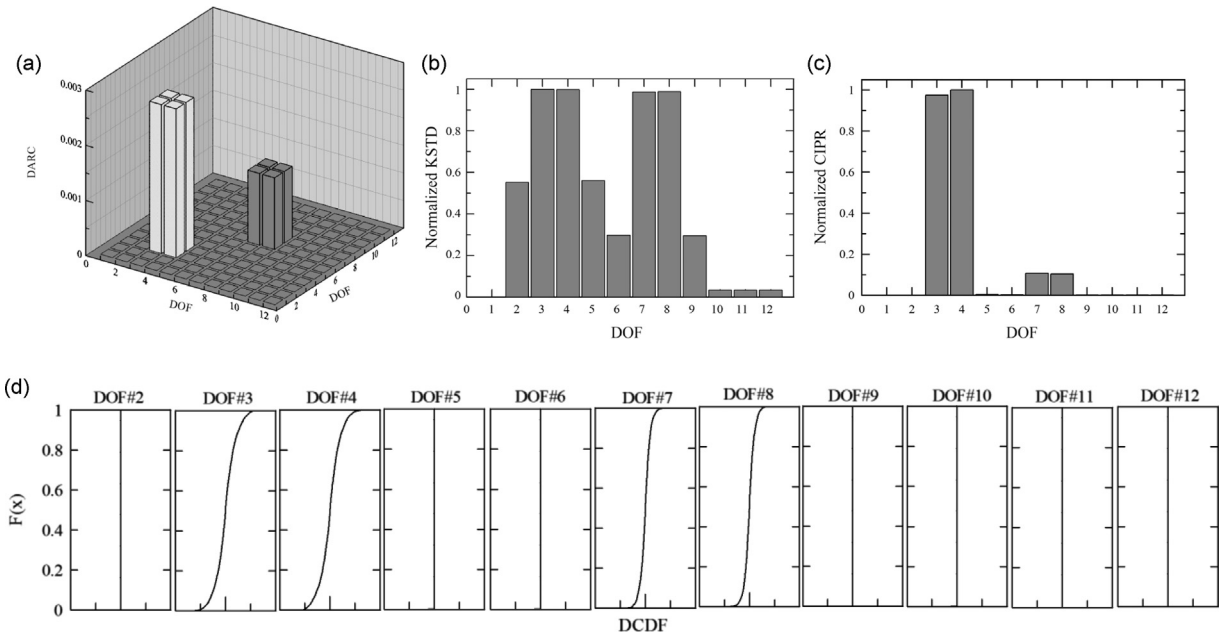

Fig. 13. DSFs of undamped shear building for damage at 4th and 8th storey levels: (a) DARC, (b) KSTD, (c) CIPR, and (d) DCDF (within -4×10^{-4} to 4×10^{-4}).

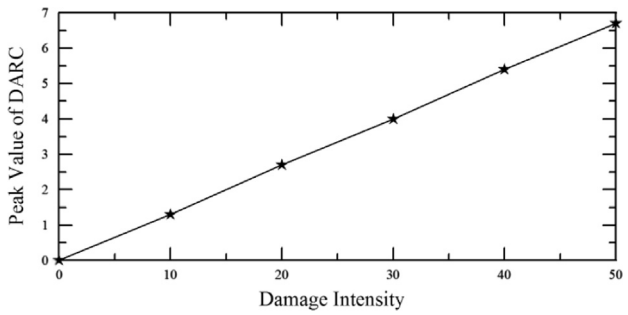

Fig. 14. Difference in first ARX model coefficients ($\times10^{-3}$) with damage intensity.

technique, which provides statistically meaningful results with a substantially small sample size. For each realization of structural stiffness, the structural responses in terms of horizontal floor accelerations were recorded and used to form the ARX model. After that, the DSFs were estimated for each realization. The mean value of each DSF is then obtained. It has been found that a sample size of 100 is enough to guarantee the convergence of mean and variance for each DSF.

Fig. 12(a)–(d) shows the plots of mean DSFs in the presence of parametric stiffness uncertainties. One can observe from Fig. 12(a) and (c) that DARC and CIPR can successfully locate the damage. However, Fig. 12(d) and (b) show uniform trend for all dofs, failing to identify any damage location. This is because the way KSTD and DCDF are evaluated from the ECDF.

4.1.3. Damage at multiple locations

To assess the efficiency of the proposed DSFs in identifying damages at multiple locations, the stiffness of the 4th and 8th storeys of the undamped shear building (Fig. 5) is reduced by 20 percent and 10 percent, respectively. A similar procedure is followed as earlier to generate the response of each dof of the undamaged and damaged models. ARX model coefficients are then determined utilizing these responses.

Fig. 13(a)–(d) shows the plot of different DSFs with dofs. One can observe from Fig. 13(a) that the difference in ARX model coefficient is more near the dof 4 and dof 8. It can also be noticed that the difference in the coefficient is relatively more at dof 4 than that in case of the dof 8. This is because the damage intensity is more at the 4th storey level when compared with that of the 8th storey level. From Fig. 13(b), one can observe that the large values occur at a few distinct locations: at dofs 3, 4 and dofs 7, 8 successfully indicating the damage locations. This DSF, however, fails to associate the intensity of damage with the amplitude of KS statistical distance. Fig. 13(c) and (d) shows that CIPR and DCDF can detect damages at two locations. However, a linear correlation cannot be observed between the damage intensity and the peak CIPR value.

4.1.4. Effect of damage intensity on DSFs

To investigate the effect of damage intensity on all the proposed DSFs (DARC, KSTD, CIPR, and DCDF), the shear building as described earlier (Fig. 5(a)) is considered along with five different damage intensities. These damage intensities represent 10 percent, 20 percent, 30 percent, 40 percent and 50 percent stiffness reduction of the 6th storey level. Fig. 14 shows a plot of peak value of DARC with damage intensity. One can notice from this figure that the peak value of DARC increases linearly with the damage intensity. This is in good agreement with Eq. (25), which was obtained by neglecting higher order terms. It is therefore clear that a first-order approximation (Eq. (25)) as derived earlier is good enough to show a linear trend of damage intensity with peak DARC even for a high intensity of damage. Thus, DARC can be used to quantify damage intensity as well.

Table 1 provides the value of KSTD with each dof for various damage intensities. It can be observed from this table that the value of KSTD for a given dof does not show any trend with damage intensity. However, for all damage intensities considered in this study, KSTD shows a good capability in damage localization, i.e., maximum values occurring near dofs 5 and 6. Therefore, KSTD can be used for damage localization only without associating with damage quantification.

Table 2 shows CIPR values for each dof with various damage intensities. From this table, it can be observed that nonzero values are found at dof 5 and dof 6 indicating the damage location (i.e., the 6th storey level). There is however no correlation between damage intensity and CIPR values and thus, CIPR cannot be used for damage quantification.

Fig. 15 shows plots of DCDF for dofs 5 and 6 with various damage intensities. Plots corresponding to other dofs are not shown in this figure for clarity of presentation. From this figure, it can be observed that a lower damage is associated with a steeper curve and thus, DCDF can be used for damage quantification.

Table 1
Variation of KSTD with damage intensity.

Damage (%)	**dof 1**	**2**	**3**	**4**	**5**	**6**	**7**	**8**	**9**	**10**	**11**	**12**
10	0	0.016	0.017	0.338	0.498	0.498	0.333	0.016	0.016	0.016	0.016	0.016
20	0	0.018	0.018	0.469	0.499	0.499	0.468	0.016	0.018	0.018	0.018	0.018
30	0	0.006	0.006	0.409	0.502	0.501	0.409	0.006	0.006	0.006	0.006	0.006
40	0	0.009	0.009	0.340	0.513	0.513	0.339	0.008	0.009	0.009	0.009	0.009
50	0	0.014	0.013	0.396	0.499	0.498	0.396	0.013	0.014	0.014	0.014	0.014

Table 2
Variation of CIPR with damage intensity.

Damage (%)	**dof 1**	**2**	**3**	**4**	**5**	**6**	**7**	**8**	**9**	**10**	**11**	**12**
10	0.000	0.000	0.000	0.000	1.000	0.976	0.000	0.000	0.000	0.000	0.000	0.000
20	0.000	0.000	0.000	0.000	1.000	0.994	0.000	0.000	0.000	0.000	0.000	0.000
30	0.000	0.000	0.000	0.000	1.000	0.932	0.000	0.000	0.000	0.000	0.000	0.000
40	0.000	0.000	0.000	0.000	1.000	0.997	0.000	0.000	0.000	0.000	0.000	0.000
50	0.000	0.000	0.000	0.000	1.000	0.998	0.000	0.000	0.000	0.000	0.000	0.000

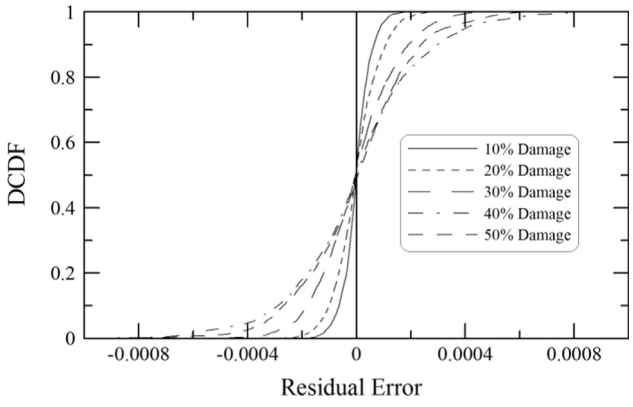

Fig. 15. DCDF with damage intensity.

4.2. Steel moment-resisting frame

To investigate the performance of the proposed DSFs in a frame building, the 12-storey SMRF as mentioned earlier is considered (Fig. 5(b)). This building [41,42] was designed using the lateral load distribution specified in the Uniform Building Code, Structural Engineering Design Provisions [43]. The fundamental period of this structure is found to be 1.54 s. Two-percent Rayleigh damping is considered for this steel structure. Table 3 provides the details of the steel sections used for modelling this SMRF. This model is developed in OpenSees [44] using beam-column elements. A uniform seismic mass of 64000 kg per floor was lumped at nodal points of each floor level in such a way that the interior nodes have twice the mass of that of the exterior nodes to simulate a realistic mass distribution. Subsequently, the structure is subjected to a band limited white-noise (with a frequency range of 0.1–25 Hz) base excitation with a sampling rate of 100 Hz and standard deviation of 0.01*g*. The damage in the structure is simulated by a stiffness reduction of 20 percent on each column of the 6th storey level. For both damaged and undamaged cases, the structural responses are evaluated using OpenSees. To simulate the response under an ambient condition, the acceleration response from each floor is recorded for 15 min by performing time history analysis. Further, the acceleration response of dof 1 is considered as input and the remaining responses as output in the framework of ARX model [27].

Fig. 16 (a)–(d) provides the plots of different DSFs (DARC, KSTD, CIPR and ECDF) with dofs. One can observe large values at dofs 5 and 6 in Fig. 16(a)–(c). Similarly, in Fig. 16(d) a discernible curve is observed at dofs 5 and 6. Thus, all the proposed DSFs are capable of locating damage. It is however important to note that large values are also observed at dof 2 in Fig. 16(a) and (c) although there is no damage in this location. This is because, in the framework of ARX, the response of dof 1 is selected as the dummy input. As a result, there is a discontinuity observed in the adjacent dof, i.e., in dof 2. This false indication is however not observed in case of KSTD and DCDF (Fig. 16(b) and (d)) due to the fact that the distribution of residual errors for the damaged and undamaged states are identical where there is no damage. Therefore, one can note that KSTD and DCDF are better indicators of damage location for frame structures.

Table 3
Steel sections used in modelling SMRF.

External column	Section	Internal column	Section	Beam	Section
C1	W14 × 176	C5	W14 × 257	B1	W30 × 124
C2	W14 × 132	C6	W14 × 211	B2	W30 × 116
C3	W14 × 109	C7	W14 × 193	B3	W30 × 108
C4	W14 × 90	C8	W14 × 159	B4	W30 × 99

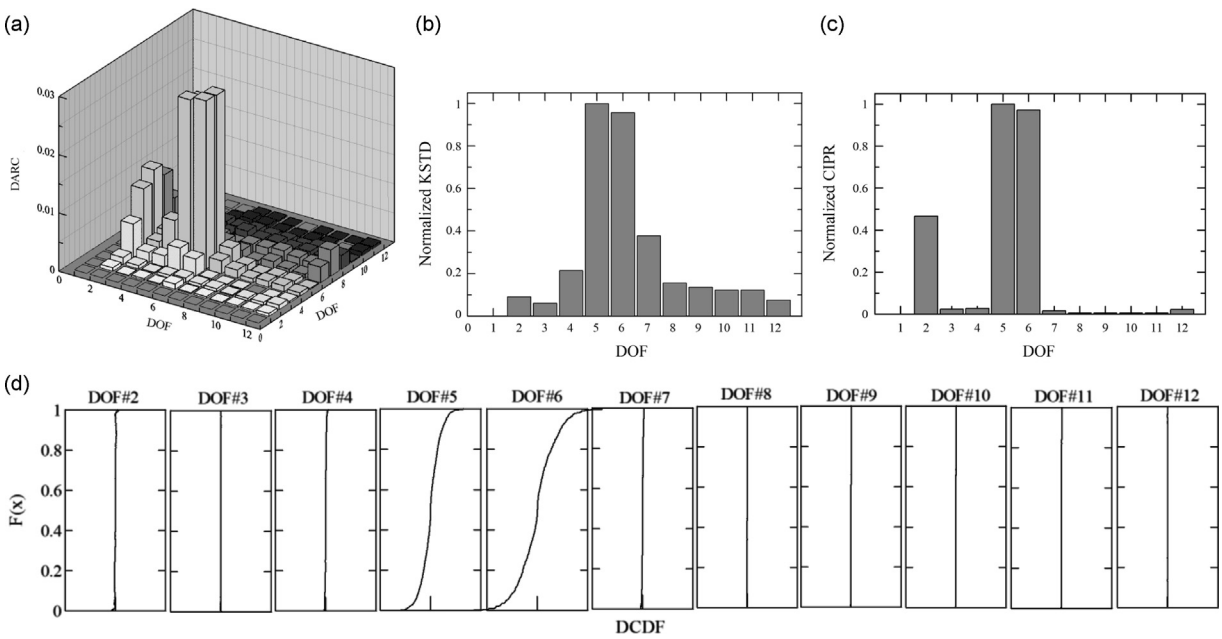

Fig. 16. DSFs in case of SMRF building for damage at the 6th floor level: (a) DARC, (b) KSTD, (c) CIPR, and (d) ECDF (within −0.01 to 0.01).

5. Comparison of the proposed DSFs with existing damage indices

In order to show the efficiency of the proposed DSFs, a summary of performance of these DSFs for various cases as discussed earlier is provided in Table 4. From this table, one can see that DARC performs well in all conditions except in the presence of measurement noise. This is because DARC is calculated directly from the time domain signal and it cannot handle noisy data properly. KSTD performs well in the presence of noise but unable to localize damage in case of higher model order, higher system damping and parametric uncertainty. Except multiple damage case, CIPR can localize damage efficiently in all conditions. Finally, DCDF is unable to localize damage in the presence of noisy measurements and parametric uncertainty. It is envisioned that this table will be of help for localizing damage under a particular situation.

Catbas et al. [45] dealt with modal flexibility-based deflection and modal curvature using multi-input–multi-output dynamic data to localize damages in experimental models. The displacement profile is obtained using load vector method to build the modal flexibility-based DSFs for damage localization. The modal curvature is found to be vulnerable with random

Table 4
Performance of DSFs under various conditions.

Case	DARC	KSTD	CIPR	DCDF
Undamped	✓	✓	✓	✓
With model order ARX(5,3)	✓	×	✓	✓
In the presence of high measurement noise	×	✓	✓	×
In the presence of high system damping	✓	×	✓	✓
In the presence of parameteric uncertainty	✓	×	✓	×
Multiple damage case	✓	✓	×	✓
SMRF	✓	✓	✓	✓
Experimental investigation	✓	✓	✓	✓

✓: Capable of detecting damage location. ×: unable to localize damage.

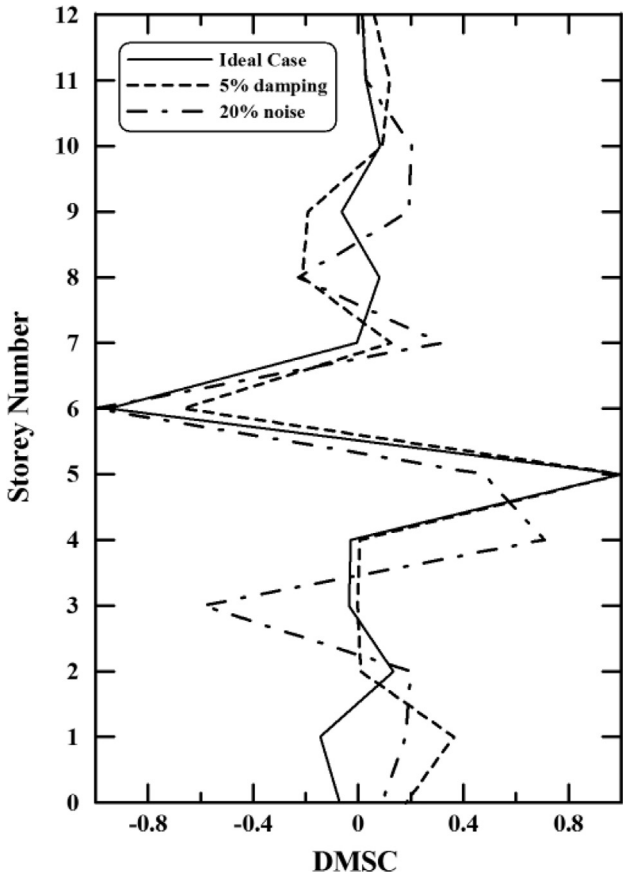

Fig. 17. Difference in mode shape curvature in structural damage localization.

noise as the derivatives of the data are estimated. According to their recommendation, these DSFs are expected to perform well, if used along with any local damage detection methodology. Nair and Kiremidjian [46] proposed a DSF based on the energies of the wavelet coefficients obtained by Haar wavelet transform and demonstrated their proposition on ASCE benchmark structure (referred earlier) under various damage environments. This DSF also requires the information of the input signal. Noh et al. [47] proposed three damage sensitive features for seismic damage quantification following strong earthquake based on wavelet energy and showed their sensitiveness for various damage patterns through experimental as well as simulation studies. Among their proposed DSFs, two of them require input ground motion information. Sinha and Shiradhonkar [48] provided a review study on various existing seismic damage detection indices to compare their performance on buildings. Almost all these damage indices either need the excitation information or require any standard reference.

This study focuses on proposing DSFs using output-only measurements. Therefore, in this section, an existing output-only time-domain damage detection technique, namely natural excitation technique (NExT-ERA) with eigensystem realization algorithm (ERA), is considered to compare the performance of these proposed DSFs with a mode shape-based feature calculated from this technique. NExT-ERA is a very popular and robust time-domain approach for damage detection. In this approach at first, NExT is employed to find out the free vibration response from ambient response assuming the input excitation to be white noise. After that, ERA is used to extract the modal parameters from free vibration response. These modal parameters can be used to identify and localize damage.

Following the studies conducted by Pandey et al. [49] and Roy and Ray-Chaudhuri [50], difference in mode shape curvature (DMSC) is taken as the feature for damage localization to compare the performance of the ARX-based DSFs proposed in this paper under various circumstances. For this purpose, the twelve-storey shear building and its damage scenario as considered earlier (shown in Fig. 5(a)) are utilized. NExT-ERA is applied on the structural response only to identify the modal parameters. After that, the damage feature, DMSC, is constructed from the mode shape using central difference method. The DMSC for various realistic condition is calculated. Fig. 17 shows the plot of difference in mode shape curvature for three conditions such as undamped condition, with 5 percent damping, and with 20 percent measurement noise. From Fig. 17, one can observe that the damage is localized efficiently. It can also be noted that the structural damping does not affect the efficiency of DMSC in damage localization, whereas the performance of this feature degrades with the presence of measurement noise. These results are consistent with the results of damage localization obtained using the proposed ARX-based set of DSFs (see Table 4).

6. Experimental verification of the proposed DSFs

To investigate the performance of the proposed set of DSFs, an experimental study involving shake table testing has been conducted on a three-dimensional scaled model (geometric scale of 1:20 approximately) of a six-storey frame. The building model has uniform storey stiffness along the height. Fig. 18(a) and (b) shows the elevation along and across the direction of shaking, respectively. Fig. 19 is the plan view of the experimental model. The plan dimensions of the model are 210 mm × 210 mm with the height of each floor being 130 mm. The columns are made up of 8 mm × 8 mm steel square sections. The beams along the direction of shaking are of 6 mm × 6 mm steel square sections. Beams made of 30 mm × 6 mm wide aluminium rectangular plates are used across the direction of shaking. The logic behind using these aluminium plates in the perpendicular direction is to support sensors and lead mass blocks. The lead mass blocks are added to all six floors to increase floor masses. The details of these masses are provided in Table 5. One can notice that the added mass on each floor is around 10.3 kg. The small variation of masses is due to slight variation of geometrical shape of the blocks.

6.1. Experimental set-up

The structure was subjected to a band-limited white noise of mild intensity base excitation to simulate ambient condition. This was achieved by mounting the structure on a uni-axial shake table, as shown in Fig. 21(a). The enlarged partial side view of the experimental model is shown in Fig. 21(b). Fig. 21(c) is the zoomed view of an accelerometer attached to any typical floor with the help of an aluminium angle section. The joints, as shown in Fig. 21(d)), were constructed in such a way that any structural elements can be replaced with another element of same length utilizing element removal arrangement. It may be

Table 5
Mass added at each floor level by using lead blocks.

Floor level	Added mass (kg)
1	10.382
2	10.293
3	10.311
4	10.364
5	10.400
6	10.350

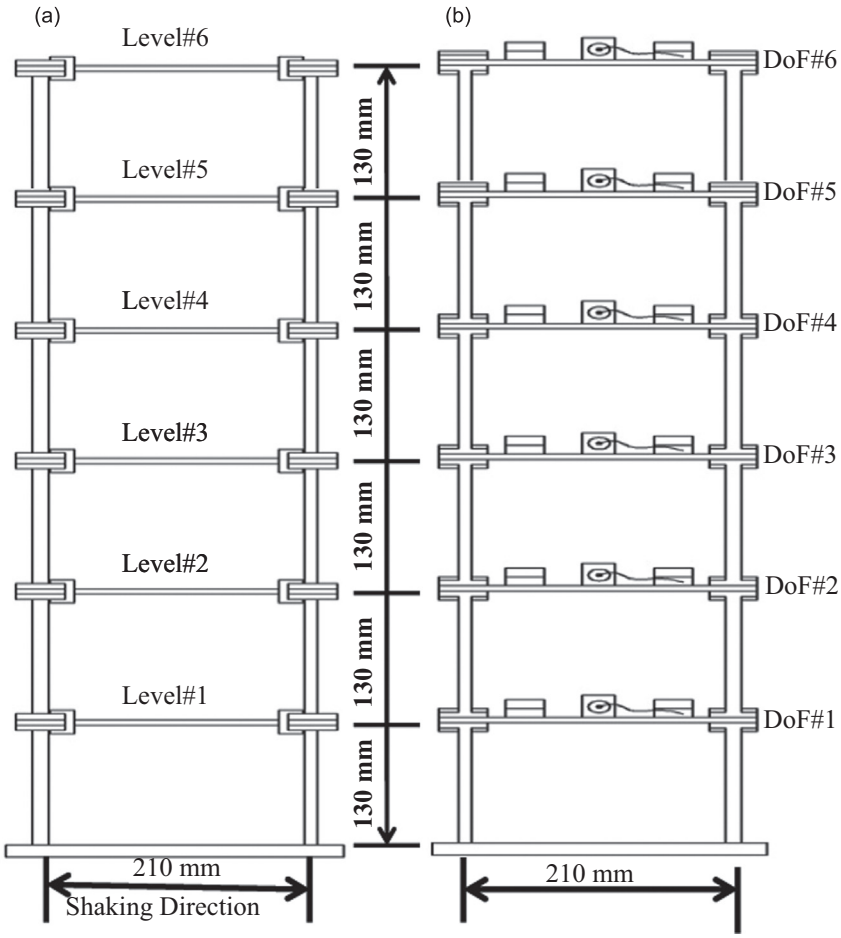

Fig. 18. Experimental model: (a) schematic elevation along the shaking direction and (b) elevation across the shaking direction.

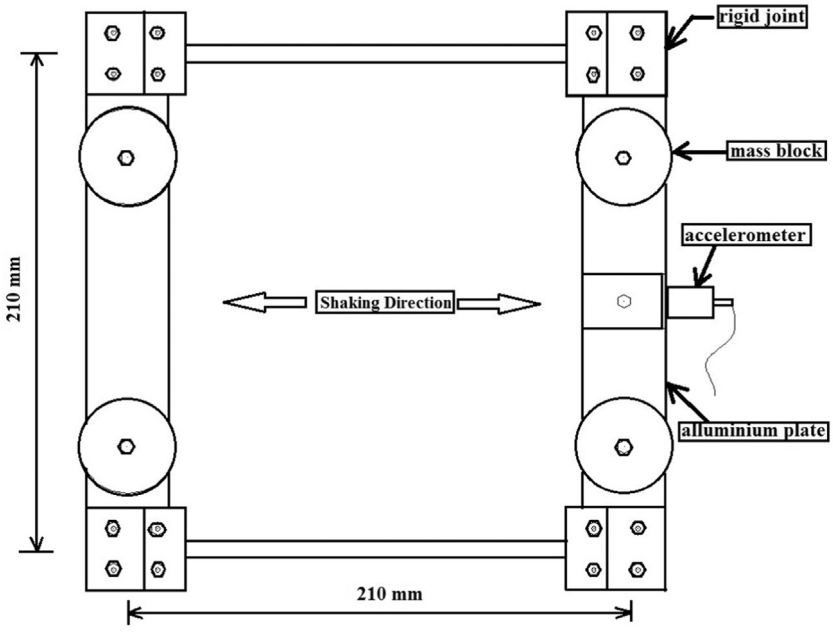

Fig. 19. Schematic plan view of the experimental model.

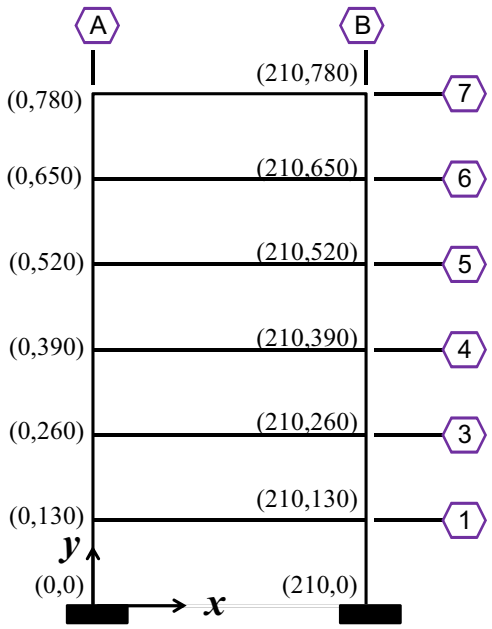

Fig. 20. Numerical Similitude modelled in SAP 2000.

noted that at any floor, one, two, three or all four columns could have been replaced. However, to achieve maximum stiffness degradation with reduced section of 6 mm × 6 mm, replacement of four columns at the 4th storey level (i.e., between dof 3 and dof 4) was adopted. A representative two-dimensional numerical model of the experimental structure along the direction of shaking is generated in SAP2000 [51], as shown in Fig. 20. The dead load and modal analyses are performed. It was found that the mass participation factor was 91.7 percent for the fundamental mode. This implies that under white-noise base-excitation, the first mode will dominate in the response.

6.2. Instrumentation and data acquisition

PCB 393B04 Seismic, miniature (50 g i.e., 0.4 percent of any typical floor approximately), ceramic flexural ICP accelerometer with a sensitivity of 1 V/g was installed at each floor level along the direction of shaking. An input signal with absolute peak acceleration of 0.01g was used as the shake table motion. The horizontal acceleration response from each floor was recorded to a data acquisition system of National Instruments PXIe-1062Q (as shown in Fig. 21(e)) through microdot cables with a sampling frequency of 1000 Hz. This sampling frequency may be too high considering the natural frequency of the model. However, this was the minimum possible sampling frequency with the data card via channel NI PXI-4472. A user friendly data-logging software LabVIEW was used to acquire data digitally.

6.3. Result and discussion

The structure was excited in healthy as well as damaged condition (with peak acceleration of 0.01g) to simulate ambient condition. Structural response in terms of horizontal floor acceleration was recorded from healthy as well as damaged structure for 5 min (i.e., 300 s). To eliminated initial transient response, first 60 s data was removed from the record. To reduce the size of the data (and hence further computation), the record was downsampled to a sampling frequency of 100 Hz using 'resample' toolbox in MATLAB. Only the fundamental mode is considered to analyse the experimental data as this is the dominant mode in response. The fundamental frequency of the experimental model is observed as 9.83 Hz. In addition, the damping ratio of the fundamental mode shape is found to be 0.27%. A 4th-order Butterworth filter with a bandpass of 0.01–25 Hz was applied to denoise the data.

The acceleration response of dof 1 is assumed as the input for the ARX model and the rest of the responses are considered as output. The ARX model coefficients and residual errors are estimated from the ARX model of the undamaged and damaged cases. The damage sensitive features (i.e., DARC, KSTD, CIPR and DCDF) are then estimated. Fig. 22(a)–(d) show the plots of DARC, KSTD, CIPR and DCDF. From Fig. 22(a), one can notice that a similar pattern as that of Fig. 8(a) is also observed here, showing the damage location between dofs 3 and 4. One can also observe from the plot of KSTD in Fig. 22(b) and CIPR in Fig. 22(c) that the largest values are occurring at dofs 3 and 4, indicating the location of damage. From Fig. 22(d), it may be observed that the difference in CDFs is more at dofs 3 and 4 to show damage at the 4th storey level. These results are quite similar to those obtained from numerical study (Table 4). Hence, using the proposed set of DSFs, one can

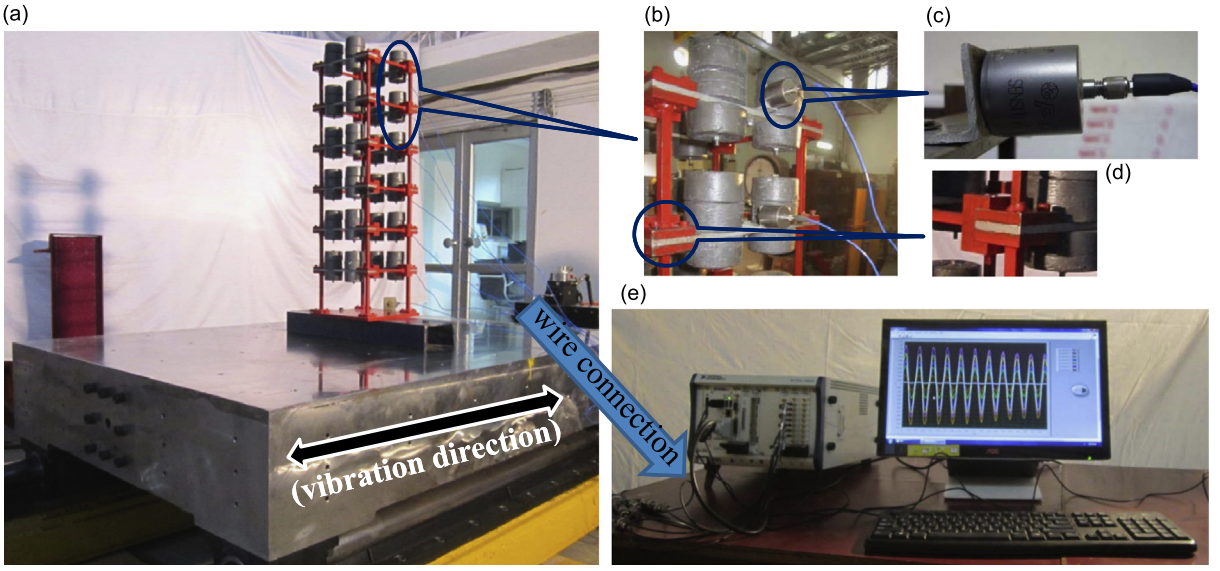

Fig. 21. Laboratory set up: (a) specimen mounted on shake table, (b) enlarged side view of the model, (c) sensor arrangement, (d) joint details and (e) circuit arrangement and data acquisition system.

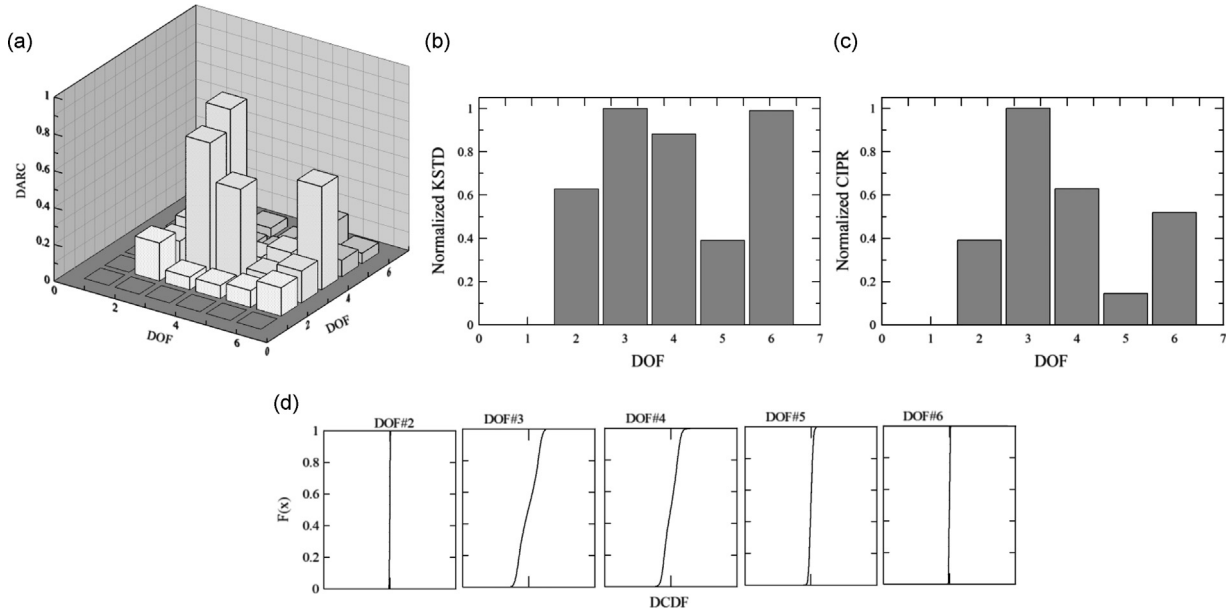

Fig. 22. DSFs from the experimental model for damage at the 4th storey level: (a) DARC, (b) KSTD, (c) CIPR, and (d) ECDF (within −0.04 to 0.04).

experimentally identify the location of damage. Perhaps the reasons behind the successfulness of all four DSFs in localizing damage are low structural damping and the absence of any significant measurement noise.

7. Conclusion

In this work, a set of four damage sensitive features (DSFs) has been proposed for structural damage localization using vibration response of output-only systems and autoregressive (ARX) model with exogenous input. These DSFs are (i) difference in first ARX model coefficients (DARC), (ii) Kolmogorov–Smirnov (KS) test statistical distance (KSTD), (iii) confidence interval to peak-pdf ratio (CIPR) of ARX model residual error, and (iv) the difference in empirical cumulative distribution functions (DCDFs) of ARX model residual error between the undamaged and damaged states. At first, to establish a relation between the change in ARX model coefficients and structural normalized stiffness, a mathematical

formulation is presented. After that, KS test parameters are described to show the sensitivity of statistical distance of autoregressive model residual error with damage location. A numerical illustration is then carried out with a shear building and a steel moment-resisting frame (SMRF). Damage in these structures is introduced in the form of stiffness degradation of different elements. To simulate the output-only conditions, the output response from a sensor is assumed as input and the response from the remaining sensors are considered as output in the framework of ARX model. A study is also conducted to understand the relation of these DSFs with damage intensity. In addition, a study is presented to compare the performance of the proposed set of DSFs with an existing popular approach of damage localization. Finally, an experimental study involving shake table testing has been carried out to investigate the performance of these DSFs for real data. Some important findings of this study are as follows:

- For undamped structure, all the proposed DSFs can accurately locate the damage. Also, in the presence of significant damping, these DSFs can also localize damage although the performance of KSTD is inferior to other DSFs in this case.
- Damage at multiple locations with different damage intensities can be identified with the proposed DSFs. However, in case of multiple damages with varying intensities, KSTD fails to associate with damage intensities.
- A study conducted using data contaminated with sensor noise shows that except DARC, all other DSFs (KSTD, CIPR and DCDF) can successfully localize damage. Also, considering uncertainty in storey stiffness, is has been found that except KSTD, all other DSFs (DARC, CIPR and DCDF) are efficient in localizing damage. Thus, the proposed set of DSFs can successfully localize damage in the presence of parametric uncertainty and measurement noise.
- It is found that DARC and DCDF show a nice trend with damage intensity, while in case of KSTD and CIPR, no such trend is observed. It is also noted that DARC shows a linear trend with damage intensity as shown mathematically by neglecting higher order terms. Thus, DARC and DCDF can be used for damage quantification, if properly calibrated.
- In case of steel moment-resisting frame, KSTD and DCDF can accurately localize damage. In addition to indicating actual damage location, DARC and CIPR show spurious large values in the vicinity of dummy input. However, this drawback of showing a false detection by DARC and CIPR in case of SMRF can be circumvented by using dummy inputs at different locations.
- From the comparison study, it has been shown that the proposed set of DSFs can localize damage efficiently as that of the DMSC approach.
- It can be observed from the experimental results that the proposed set of DSFs is good enough to identify the damage location.

In general, it is concluded that the proposed set of DSFs, when used together, can satisfactorily localize damage in the presence of damping, multiple damages, noise, and parametric uncertainties. It may also be noted that apart from the computation required for ARX model, evaluation of these DSFs does not involve significant additional calculation. As in the case of ambient excitation, it is very difficult and sometimes impossible to obtain information of the input, one of the outputs is taken as input to develop ARX model. The only drawback of this approach is that the damage cannot be localized for the location where this input is acted upon. To circumvent this issue, it has been suggested to repeat the procedure with two or more different input location. It may also be noted (based on further analysis) that with uncorrelated white-noise at each floor, this algorithm will not work. It may however be kept in mind that in real-world scenario, there are mainly two sources of ambient excitation: (i) background excitation (e.g., internal excitation due to occupants, running machinery etc., and base excitation due to seismic activity, traffic movement nearby, etc.) and (ii) wind excitation. In case of base excitation, the input of each floor is correlated as the influence coefficient is unity for each floor mass (sometimes known as uniform excitation). For wind excitation, it has been shown in the literature that the correlation drops with distance or height. If the building is very tall, perhaps the correlation will be lost between the top and bottom floors. However, for nearby floors, the correlation of excitation will exist. Hence, it is envisioned that the proposed framework will provide desired results. Perhaps tests on a full scale structure can be performed in the future to study this aspect.

Acknowledgements

The authors gratefully acknowledge the travel support of UKIERI (UKIERI/MDeS/20120045) for disseminating some of the works at the University of Sheffield, Sheffield, UK and obtain valuable inputs from Profs. K Visakan and S. Anderson. The authors appreciate the logistic support provided by the Structural Engineering Laboratory, IIT Kanpur for smooth conduction of the experiment.

References

[1] R. Brincker, L. Zhang, P. Andersen, Modal identification of output-only systems using frequency domain decomposition, *Smart Materials and Structures* 10 (3) (2001) 441.
[2] J.M. Caicedo, S.J. Dyke, E.A. Johnson, Natural excitation technique and eigensystem realization algorithm for phase I of the IASC-ASCE Benchmark Problem: *simulated data*, *Journal of Engineering Mechanics, ASCE* 130 (1) (2004) 49–60.
[3] S.R. Ibrahim, Random decrement technique for modal identification of structures, *Journal of Spacecraft and Rockets* 14 (1977) 696–700.
[4] H. Sohn, C.R. Farrar, Damage diagnosis using time series analysis of vibration signals, *Smart Materials and Structures* 10 (3) (2001) 1–6.

[5] A. Cheung, C. Cabrera, P. Sarabandi, K.K. Nair, A. Kiremidjian, H. Wenzel, The application of statistical pattern recognition methods for damage detection to field data, *Smart Materials and Structures* 17 (6) (2008) 065023.
[6] S. Anderson, P. Aram, B. Bhattacharya, V. Kadirkamanathan, Analysis of composite plate dynamics using spatial maps of frequency domain features described by gaussian processes, *Advances in Control and Optimization of Dynamics Systems, IFAC*, 2014.
[7] J.N. Wandji, A nonparametric goodness-of-fit test for a class of parametric autoregressive models, *Journal of Statistical Planning and Inference* 71 (1–2) (1998) 57–74.
[8] K. Worden, G. Manson, N.R.J. Fieller, Damage detection using outlier analysis, *Journal of Sound and Vibration* 229 (3) (2000) 647–667.
[9] C. Kar, A.R. Mohanty, Application of KS test in ball bearing fault diagnosis, *Journal of Sound and Vibration* 269 (1–2) (2004) 439–454.
[10] S.G. Mattson, S.M. Pandit, Statistical moments of autoregressive model residuals for damage localisation, *Mechanical Systems and Signal Processing* 20 (3) (2006) 627–645.
[11] C. Kar, A.R. Mohanty, Multistage gearbox condition monitoring using motor current signature analysis and Kolmogorov–Smirnov test, *Journal of Sound and Vibration* 290 (1–2) (2006) 337–368.
[12] S. Da Silva, M.D. Junior, V.L. Junior, Structural health monitoring in smart structures through time series analysis, *Structural Health Monitoring: An International Journal* 7 (September (3)) (2008) 231–244.
[13] H. Zheng, A. Mita, Localized damage detection of structures subject to multiple ambient excitations using two distance measures for autoregressive models, *Structural Health Monitoring: An International Journal* 8 (May (3)) (2009) 207–222.
[14] B. Iser, G. Schmidt, W. Minker, *Bandwidth Extension of Speech Signals*, Springer, New York, NY, USA, 2008.
[15] D. Bachmann, H. Dette, A note on the Bickel–Rosenblatt test in autoregressive time series, *Statistics and Probability Letters* 74 (3) (2005) 221–234. ISSN 0167-7152.
[16] S. Na, Goodness-of-fit test using residuals in infinite-order autoregressive models, *Journal of the Korean Statistical Society* 38 (3) (2009) 287–295.
[17] F. Gao, Y. Lu, An acceleration residual generation approach for structural damage identification, *Journal of Sound and Vibration* 319 (1–2) (2009) 163–181.
[18] X. Wang, V. Makis, Autoregressive model-based gear shaft fault diagnosis using the Kolmogorov–Smirnov test, *Journal of Sound and Vibration* 327 (3–5) (2009) 413–423.
[19] Y. Dong, Y. Li, M. Lai, Structural damage detection using empirical-mode decomposition and vector autoregressive moving average model, *Soil Dynamics and Earthquake Engineering* 30 (3) (2010) 133–145.
[20] D. Bernal, D. Zonta, M. Pozzi, ARX residuals in damage detection, *Structural Control and Health Monitoring* 19 (4) (2011) 535–547.
[21] A.A. Mosavi, D. Dickey, R. Seracino, S. Rizkalla, Identifying damage locations under ambient vibrations utilizing vector autoregressive models and Mahalanobis distances, *Mechanical Systems and Signal Processing* 26 (2012) 254–267.
[22] Y. Zhan, C.K. Mechefske, Robust detection of gearbox deterioration using compromised autoregressive modeling and Kolmogorov–Smirnov test statistic. Part I: *compromised autoregressive modeling with the aid of hypothesis tests and simulation analysis*, *Mechanical Systems and Signal Processing* 21 (5) (2007) 1953–1982.
[23] Y. Zhan, C.K. Mechefske, Robust detection of gearbox deterioration using compromised autoregressive modeling and Kolmogorov–Smirnov test statistic. Part II: *experiment and application*, *Mechanical Systems and Signal Processing* 21 (5) (2007) 1983–2011.
[24] K. Roy, S. Ray-Chaudhuri, Autoregressive model for structural condition assessment in presence of parametric uncertainty, *Proceeding of the International Symposium on Engineering under Uncertainty: Safety Assessment and Management*, BESU, Shibpur, India, January 2012.
[25] S. Thanagasundram, S. Spurgeon, F.S. Schlindwein, A fault detection tool using analysis from an autoregressive model pole trajectory, *Journal of Sound and Vibration* 317 (3–5) (2008) 975–993.
[26] S.M. Kay Jr., S.L. Marple, Spectrum analysis—a modern perspective, *Proceedings of IEEE* 69 (11) (1981) 1380–1419.
[27] Y. Lu, F. Gao, A novel time-domain auto-regressive model for structural damage diagnosis, *Journal of Sound and Vibration* 283 (3–5) (2005) 1031–1049.
[28] S. Lee, A note on the residual empirical process in autoregressive models, *Statistics & Probability Letters* 32 (4) (1997) 405–411.
[29] L. Meirovitch, *Fundamentals of Vibrations*, McGraw-Hill International Edition, Mechanical Engineering Series, New York, NY, USA, 2001.
[30] R. Villaverde, *Fundamental of Earthquake Engineering*, CRC Press, Taylor and Francis Group, Boca Raton, FL, 2009.
[31] C. Soize, A comprehensive overview of a non-parametric probabilistic approach of model uncertainties for predictive models in structural dynamics, *Journal of Sound and Vibration* 288 (3) (2005) 623–652.
[32] P.H. Prasthofer, C.W. Beadle, Dynamic response of structures with statistical uncertainties in their stiffnesses, *Journal of Sound and Vibration* 42 (4) (1975) 477–493.
[33] B. Segui, B. Faverjon, G. Jacquet-Richardet, Effects of random stiffness variations in multistage rotors using the polynomial chaos expansion, *Journal of Sound and Vibration* 332 (18) (2013) 4178–4192.
[34] Y.L. Xu, J. Zhang, J. Li, X.M. Wang, Stochastic damage detection method for building structures with parametric uncertainties, *Journal of Sound and Vibration* 330 (20) (2011) 4725–4737.
[35] K. Zhang, H. Li, Z. Duan, S.S. Law, A probabilistic damage identification approach for structures with uncertainties under unknown input, *Mechanical Systems and Signal Processing* 25 (4) (2011) 1126–1145.
[36] M. Chandrashekhar, R. Ganguli, Damage assessment of structures with uncertainty by using mode-shape curvatures and fuzzy logic, *Journal of Sound and Vibration* 326 (3–5) (2009) 939–957.
[37] J.E. Mottershead, M. Link, M.I. Friswell, The sensitivity method in finite element model updating: *a tutorial*, *Mechanical Systems and Signal Processing* 25 (7) (2011) 2275–2296.
[38] Y. Ma, Z. Liang, M. Chen, J. Hong, Interval analysis of rotor dynamic response with uncertain parameters, *Journal of Sound and Vibration* 332 (16) (2013) 3869–3880.
[39] G.J. Savage, Y.K. Son, Frequency response design of uncertain systems using performance indices and meta-models, *Journal of Sound and Vibration* 332 (26) (2013) 6949–6967.
[40] B. Minasny, A.B. McBratney, A conditioned Latin hypercube method for sampling in the presence of ancillary information, *Computers & Geosciences* 32 (9) (2006) 1378–1388.
[41] P.R. Santa-Ana, E. Miranda, Strength reduction factors for multi-degree-of-freedom systems, *Proceedings of the Twelfth World Conference on Earthquake Engineering*, Auckland, New Zealand, Vol. 1446, 2000, p. 8.
[42] S. Ray Chaudhuri, R. Villaverde, Effect of building nonlinearity on seismic response of nonstructural components: *a parametric study*, *ASCE Journal of Structural Engineering* 134 (4) (2008) 661–670.
[43] Uniform Building Code, Structural engineering design provisions, *International Conference of Building Officials*, Vol. 2, Whittier, California, 1994.
[44] Pacific Earthquake Engineering (PEER) Center, Open system for earthquake engineering simulation, URL ⟨http://opensees.berkeley.edu/OpenSees/copyright.php⟩.
[45] F.N. Catbas, M. Gul, J.L. Burkett, Conceptual damage-sensitive features for structural health monitoring: *laboratory and field demonstrations*, *Mechanical Systems and Signal Processing* 22 (7) (2008) 1650–1669.
[46] K.K. Nair, A.S. Kiremidjian, Derivation of a damage sensitive feature using the Haar wavelet transform, *Journal of Applied Mechanics, ASME* 76 (6) (2009) 23. 061015–061015-9.
[47] H.Y. Noh, K.K. Nair, D.G. Lignos, A.S. Kiremidjian, Use of wavelet-based damage-sensitive features for structural damage diagnosis using strong motion data, *Journal of Structural Engineering, ASCE* 137 (10) (2011) 1215–1228.
[48] R. Sinha, S. Shiradhonkar, Seismic damage index for classification of structural damage - closing the loop, *Proceedings of the Fifteenth World Conference on Earthquake Engineering*, Auckland, New Zealand, 2012.

[49] A.K. Pandey, M. Biswas, M.M. Samman, Damage detection from changes in curvature mode shapes, *Journal of Sound and Vibration* 145 (2) (1991) 321–332.
[50] K. Roy, S. Ray-Chaudhuri, Fundamental mode shape and its derivatives in structural damage localization, *Journal of Sound and Vibration* 332 (21) (2013) 5584–5593.
[51] SAP2000 v14. Computers and Structures, Inc. (CSI). URL ⟨http://www.csiamerica.com/⟩.